공학석사 학위논문

Study on the PCET process of Tyrosine-rich peptide/manganese oxide hybrid film

펩타이드/무기물 복합 필름의 전도 현상 중 수소 이온과 전자의 상호작용에 관한 연구

2019 년 2 월

서울대학교 대학원

재료공학부

주 미 송

Abstract

Study on the PCET process of Tyrosine-rich peptide/manganese oxide hybrid film

Misong Ju

Department of Materials Science and Engineering

The Graduate School

Seoul National University

The control of protons and electrons transfer by proton-coupled electron transfer mechanism, called PCET, is ubiquitous in biological systems. PCET can occur in either orthogonal or collinear pathway and PCET can occur by concerted proton electron transfer or sequential proton and electron transfer pathway. The redox cofactors controlling the coupled long-range electron and short-range proton transfer in living organisms are usually amino acid side chains with acid/base or

other functionalities in protein/peptide complexes. Among various amino acids, nature has taken tyrosine as an important redox-active cofactor in diverse reactions. The most representative PCET reaction of tyrosine can be found in light reaction photosynthesis where tyrosine mediates electron transfer from Mn_4Ca cluster to the central chlorophyll P_{680} while the phenolic proton of tyrosine deprotonates to the hydrogen-bonded histidine. By this special PCET process, the rate of electron transfer from Mn_4Ca to P_{680} becomes 200 times much faster compared to the rate when there is no proton transfer process coupled to the electron transfer.

In the past, the development of electrical devices had mainly focused on controlling electronic currents. These days, however, lot of efforts are ongoing for protonic devices as ions or protons are more appropriate language involved in many electrical signaling pathway of biological system. Furthermore, when considering the highly efficient charge transfer pathway in nature, developing PCET systems and controlling their charge transport properties may be a key for the next generation devices. Inspired from the amazing tyrosine's role in nature, the ability to utilize coupled proton and electron transfer process, our group recently developed a hybrid film with a short tyrosine-rich peptide sequence. By inducing dityrosine cross-linking with the oxidant potassium permanganate, the hybridization of the peptide film and the hydrophilic manganese oxides occurred and the higher conductivity compared to other biomaterials working at room temperature was observed, showing a possibility in future bioelectronics application. In addition, the hybrid film

exhibited a high KIE 3.3 while conventional proton hopping mechanism shows KIE around 1.4. We assume that another pathway, which we expect to be PCET according to the natural system, is involved in proton transfer over conventional proton hopping. KIE for the PCET process has been studied with series of model reactions and has been discovered to cover wide range depending on factors such as temperature, reorganization energy and equilibrium proton donor-acceptor distance. Thus, prior to the practical application, the studies on charge transfer pathway and comprehensive knowledge should be proceeded.

A simultaneous ion and electron conduction is observed in inorganic materials called mixed ion-electron conductors (MIECs). MIECs have been studied for a long time and it has been found out that the law of independent migration for charge carriers is not always the case, varying with its thermodynamic state including temperature and nonstoichiometry. Several studies reported the quantified electron and ion interference effect by obtaining Onsager coefficients experimentally. According to the linear transport theory, Onsager coefficients relates the flux of a charge carrier with the driving force of all other charge carriers. For system having two charge carriers, four transport parameters were defined with Onsager coefficients. By measuring and controlling partial currents and the electrochemical potential gradients, studies got four transport parameters and accordingly Onsager coefficients in various oxide MIECs and they quantified and interpreted the interference effect among charge carriers.

In large sense, mixed ion and electron conduction includes PCET, therefore, making it possible for us to take inorganic system as a research platform for the verification and quantification of large scale PCET. Here, we investigated the proton and electron coupled transfer in the tyrosine-rich peptide/manganese oxide hybrid film by applying the concept 'Onsager coefficients' and 'transport parameters'. In this study, we propose a new paradigm to confirm and quantify PCET process of bulk materials. With the fabricated proton blocking mode sample analogous to the inorganic materials cell which block the ion movement by current flowing platinum electrodes, the electrochemical potential of protons counterbalancing the driving force of proton movement due to the coupling with electrons inside the hybrid film was measured with the Nafion membrane, the state of art proton conductor. Two transport parameters were calculated with the cell that block the transport of protons at electrodes at both ends, enabling the direct observation of one proton and one electron coupled transfer of the macroscopic film sample. In addition, the investigation on the isotope effect, replacing proton to deuterium, also supported the interference among protons and electrons in the hybrid film.

Keywords: Proton-Coupled Electron Transfer, Mixed Ion-Electron Conductors, Onsager coefficients, Nafion, Transport parameters, Tyrosine-rich peptide/manganese oxide hybrid film

Student Number: 2017-24715

Contents

List of Tables

oxygen vacancies and protons at specific positions.

List of Figures

maquette *peptide A* : Backbone sequence and peptide folding induces π -π stacking of tyrosine and histidine and indirect hydrogen bonding with water molecules. Reproduced with permission.[4] Copyright 2015, American Chemical Society. (b) Artificial photosynthetic center *triad-1*. Upon irradiation (1), the system undergoes primary electron transfer (2) and a PCET reaction (3). Reproduced with permission.[5] Copyright 2014, Nature Publishing Group.

Figure 1.2.1 YYACAYY/MnOx hybrid film. The characteristics and unique properties were analyzed by various methods. (a) AFM image of the hybrid film showing a rough surface of the hybrid film. (b) The clear dityrosine formation was observed by photoluminescence spectrum. From the 280nm excitation and the resultant emission at 305nm which is the characteristic of tyrosine, its intensity decreased by increasing $KMnO_4$ treatment concentration. From 350nm excitation and the resulting emission at 410-415nm, the characteristic of dityrosine showed the formation of an extended conjugate system by dityrosine with increasing $KMnO_4$ treatment concentration. (c) Mn 2p XPS spectrum, showing the high valence Mn^{7+} reduction into reduced species in the hybrid film, dominantly Mn^{2+} and Mn^{3+}. (d) Nyquist plots measured from gold electrode two-terminal hybrid film device by impedance spectroscopy depending on the relative humidity. The

semicircle and the inclined tail is a typical shape of proton conductors which in contact with ion blocking electrodes. The dependency on the relative humidity indicates the main charge carrier of the hybrid film is proton from water vapor. Reproduced with permission.[6] Copyright 2017, John Wiley & Sons, Inc.

Figure 1.3.1 Common scheme of oxide MIECs sample to get four Onsager coefficients. Probes 1, $1'$, 2, and $2'$ are to give a fixed value of current to the sample while probes 3, $3'$ and 4, $4'$ are to measure the electrochemical potential of electrons and ions, respectively. Platinum electrodes are shown in dark navy line and porous Pt electrodes are shown in dark navy dashed line. For the oxide MIEC which conducts electrons and doubly charged oxygen vacancies, $V_O^{\bullet\bullet}$, Yttria Stabilized Zirconia(Y_2O_3-doped ZrO_2) is used as an electron blocking electrode which block the net electronic flow in the sample and measure the chemical potential of $V_O^{\bullet\bullet}$ at 4 and $4'$ positions for both electron blocking and ion blocking mode. When flowing current through 1 and $1'$, it becomes 'electron blocking mode' as YSZ at both ends of the specimen block electronic current to flow between 1 and $1'$. When flowing current through 2 and $2'$, it becomes 'ion blocking mode' as porous Pt blocks $V_O^{\bullet\bullet}$ movement at both ends of the sample.

Figure 1.3.2 The responses of fabricated cell for CeO_2 conducting electrons and $V_O^{\bullet\bullet}$. (a) The figure shows the U and V vs. time in the ion blocking mode, indicating the ion and electron's electrochemical potential, respectively. When the current is on, U relaxes to a finite value which is not 0 while V almost immediately takes a steady state value. When the current is off, both U and V decay to zero and when the current passes in the opposite direction, it shows the same amount of variation with the first region (current > 0) but only in the opposite sign. (b) When a constant current flows in the electron blocking mode, the similar response to the U in the ion blocking mode is observed for V which relaxes to the non-zero finite value. Both results from (a) and (b) indicates the significant interference effect among ions and electrons. Reproduced with permission.[7] Copyright 2008, The Electrical Society.

Figure 1.3.3 The fluxes in a MIEC conducting e^-, $V_O^{\bullet}$, $V_O^{\bullet\bullet}$. (a) When the electrode can conduct electrons and block material transfer through the electrode, electrochemical reactions at equilibrium take place in both anode and cathode. Under steady state, the net result is that electrons are transferred by doubly charged oxygen vacancies $V_O^{\bullet\bullet}$ from the cathode to the anode in addition to the electron current through the oxide. (b) When the electrode blocks electron transfer and conducts

$V_O^{\bullet\bullet}$, electrochemical reaction takes place at the YSZ/MIEC interface . At the anode side, some of $V_O^{\bullet\bullet}$ defects are reduced to $V_O^{\bullet}$ while at the cathode side the inverse reaction occurs. The electron which reduces $V_O^{\bullet\bullet}$ into $V_O^{\bullet}$ are generated from the cathode which flow through the MIEC from the cathode to the anode. Reproduced with permission.[8] Copyright 2014, Royal Society of Chemistry.

Figure 2.3.1 Schematic diagram and a real image of the sample fabricated into proton blocking mode system. Two gold electrodes are placed outer side while two Nafion membrane electrodes are placed inside with 1mm distance between electrodes. The proton blocking mode experiment was conducted by applying a fixed voltage on outer gold electrodes and measuring U from Nafion membranes and V from gold electrodes. The positions of all probes were kept close to the center of each electrode during the measurement.

Figure 2.3.2 Nafion voltage according to the applied voltage on gold electrodes. The graph shows the linear relation between Nafion and gold voltages, indicating the interference among protons and electrons does not change regardless of applied voltage values.

Figure 2.3.3 A result of fabricated proton blocking mode system of the hybrid film at 90% RH room temperature. The voltage applying regions are

colored in yellow and orange, for each +0.6V and -0.6V. As clearly seen in the figure, the U measured from Nafion membranes on the hybrid film saturates to the finite value far from zero when applying gold voltages, indicating the significant interference effect of electrons and protons on their movement. The amount of change of voltage U is almost the same for oppositely applied voltage.

Figure 2.3.4 The voltages measured from inner electrodes when they are replaced with gold instead of Nafion. The experiment was held in order to confirm that Nafion voltage does not measure the electrochemical potential of electrons developed by the applied voltage at the outer gold electrodes. The measurement was conducted with samples having similar current level at various relative humidity ranging from 40 to 90% and the same voltage 0.6V was applied. As clearly shown in the figure, voltages from inner gold electrodes does not change according the relative humidity.

Figure 2.3.5 The responses of fabricated proton blocking mode at 60% RH using IGZO and Si wafer as non-proton conducting materials. (a) The Nafion voltage measured from the IGZO with changing the outer gold electrodes voltage in the order. There is no significant change in Nafion voltage with the change of gold voltages. (b) The Nafion voltage measured from the Si wafer. There is also no significant

change found in Nafion voltage and the size of offset is similar to the IGZO case, implying that the origin of offset does not depend on the substrate.

Figure 2.3.6 Transport parameters of the hybrid film at various humidity conditions ranging from 40 to 90% RH at room temperature. (a) The transport parameter α_i^* has a value approximately 1 at 50 to 90% RH while showing a low value near 0.5 at 40% RH. The observation of the value 1 indicates that one proton conduction is coupled to the one electron conduction, showing the proton-coupled electron transfer process in the macroscopic hybrid film. The decrease of the value implies PCET is not significant at low humidity assumingly due to the decreased hydrogen bonding network, which facilitate the PCET. (b) The transport parameter σ_e' increases with the increasing relative humidity. The result also demonstrates that protons modulated by humidity do affect the conduction of electrons, which is PCET.

Figure 2.3.7 Transport parameters of samples humidified with H_2O(black line) and D_2O(blue line) vapor. (a) The transport parameter α_i^* of either operation has a similar value at the wide range of relative humidity. The result demonstrates that significant interference also exists

between the conduction of deuterium and electron. (b) The transport parameter σ_e' of either condition is affected by relative humidity, decreasing with decreasing humidity. The electronic conductivity σ_e' with the film humidified with H_2O vapor is slightly higher than that of the film humidified with D_2O vapor. This can be interpreted as the effect of different ion mobility as a result of two times heavier mass of deuterium, affecting the conduction of surrounding electrons to be much slower.

Chapter 1. Introduction

1.1 Proton-coupled Electron Transfer of Tyrosine

1.1.1 PCET of tyrosine in nature

Precise control of proton and electron conduction plays an essential role in energy conversion process of living organisms including photosynthesis and respiration and the key components to manipulate or link electrons and protons transfer are redox-active complex in peptide/protein matrices.[9] In the light reactions photosynthesis, for instance, electron transport chain which consists of redox cofactors embedded in a protein matrix mediates long range electron transfer from water molecules to $NADP^+$, at the same time creating an electrochemical proton gradient which is involved in producing adenosine triphosphate, the main energy source of living cells.[10] In addition, in the photosystem II reaction center, while an electron is transferred from oxygen evolving center (OEC) to the central chlorophyll P_{680}, amino acid tyrosine, denoted as Tyr_z, in OEC plays a critical role as a redox intermediate between Mn_4Ca cluster catalyst in OEC and P_{680}. As shown in Figure 1.1.1 (a), Tyr_z is oxidized to transfer electrons from the Mn_4Ca cluster to P_{680}, and

this accompanies the deprotonation of a phenol residue to a hydrogen-bonded histidine having imidazole functional group which acts as a proton acceptor, resulting in the formation of neutral tyrosine radical. This process facilitates electron transfer from water molecules to P_{680} and also prevents the recombination of excited electrons and holes in P_{680}, followed by successful and effective transport of electrons to the electron transport chain.[1,4]

Commonly, electron transfer reactions in biological systems are coupled to proton transfer reactions, the basic mechanism of chemical and bio-energy conversion. This is because the coupling of electron and proton conduction between a donor and an acceptor can avoid high-energy intermediates, creating low-cost highly efficient charge transport pathways.[11] The coupling of these two charge carriers are known as proton-coupled electron transfer (PCET) and it is a very important key process in nature with utilizing the acid/base functionality of proteins/peptides amino acid side chains. For example, if there is no nearby hydrogen-bonded histidine in the photosystem II which can accept protons from Tyr_Z., the rate of electron transfer from OEC to P_{680} becomes 200 times much lower compared to the rate when hydrogen bonded histidine exists.[1]

Among various amino acids constructing complex peptide/protein assemblies, tyrosine particularly acts as a redox-active cofactor in many PCET process of nature due to its phenolic functional group. The phenolic group on tyrosine not only contributes to the structure of peptide/protein assemblies with π-π

interactions in various directions, hydrogen bonding of phenol residues or dityrosine cross-linking, but also contributes to the efficient charge transport pathway by PCET mechanism.[3] Figure 1.1.2 shows the thermodynamic cycle of the PCET of tyrosine radical formation and a conceptual reaction coordinate diagram for the PCET process. As shown in the Figure 1.1.2 (a) the pK_a values of tyrosine oxidation reactions are in the range of 10 to –2, meaning that the oxidation of tyrosine is coupled to the proton transfer reaction at most pH values.[12] Therefore, PCET of tyrosine can be widely utilized when surrounded by hydrogen bonded proton acceptors and, in fact, there are lot of examples that tyrosine mediates PCET reactions in existing biological systems, including photosystem II, ribonucleotide reductase, or blue light receptor proteins.[1,2,13–15]

In general, PCET includes not only a concerted proton and electron transfer (CPET) but also consecutive steps of PTET (proton transfer electron transfer) or vice versa (electron transfer proton transfer, ETPT). Among them, CPET is the most effective way as the process avoids the formation of charged tyrosine species by lower energy, single-step reaction, depicted in Figure 1.1.2 (b). Analogous to the electron transfer reaction which is normally described by the Marcus theory, CPET also can be viewed as tunneling of electrons and protons at the same transition state.

$$k_{CPET} = \frac{2\pi}{\hbar} V_{CPET}^2 (4\pi\ \lambda RT)^{-1/2} \exp\left(-\frac{(\Delta G^{\circ}_{CPET} + \lambda)^2}{4\lambda RT} \right)$$

where $V_{CPET} = V_{ET} \times V_{PT}$ (1)

Equation 1 shows the rate constant of CPET analogous to the rate constant of electron transfer reaction explained by Marcus theory. ΔG°_{CPET} is the free energy of the CPET reaction and λ is the reorganization energy of the nuclear configuration to form the transition state from the equilibrium state in the reaction diagram. Every parameter is affected not only by electrons but also by protons, for instance, V_{CPET}, the combined vibronic coupling of the CPET process is the product of electronic coupling (V_{ET}) and protonic coupling (V_{PT}).[1,3,16,17]

PCET has no specific directional property. In case of ribonucleotide reductase which provides all organisms with $2'$ deoxyribonuclotides for DNA synthesis, both orthogonal and collinear PCET make it possible for radical on tyrosine to be transferred to cysteine over the distance of 35Å.[13] The most important factor determining the nature of PCET is hydrogen bonding which can support long range proton conduction. The hydrogen bonding between tyrosine residues and surrounding amino acid residues governs the overlap between the donor and acceptor proton vibrational wave functions which is strongly affected by the proton transfer distance. Thus, the PCET pathway strongly depends on noncovalent interactions in proteins that can modify the overall geometry and hydrogen bonding environment.[4,15,18] For BLUF photoreceptors, the blue light sensor protein using small flavin which is responsible for photoadaptive responses of prokaryotes, PCET occurs from tyrosine to flavin and form neutral flavin/tyrosine radical pair. The BLUF domain can be reversibly switched from a light-adapted state to a dark-

adapted state which shows two different hydrogen bonding environment, leading to two different ways of PCET process. In the light-adapted state the radical pair is formed by CPET whereas in the dark-adapted state PCET occurs by sequential ETPT as a consequence of hydrogen bonding switching between the flavin and its surrounding amino acids that create a setup for proton transfer.[15] Another example showing the importance of hydrogen bonding environment can be found in another tyrosine Tyr_D in Figure 1.1.1 (b) which is located in a relatively hydrophobic domain in contrast to Tyr_z in a more hydrophilic environment of the photosystem II. Tyr_D forms a short hydrogen bond with the imidazole nitrogen atom of a nearby histidine and what distinguish Tyr_z and Tyr_D is the position of bound water molecules and the distance from the center of OEC. While the Tyr_z radical is directly involved in the water oxidation process, Tyr_D radical formed by photo-oxidation whose function is not well known is not involved in the water oxidation process and have extraordinarily long lifetime which even reaches several hours compared to the short living Tyr_z.[2]

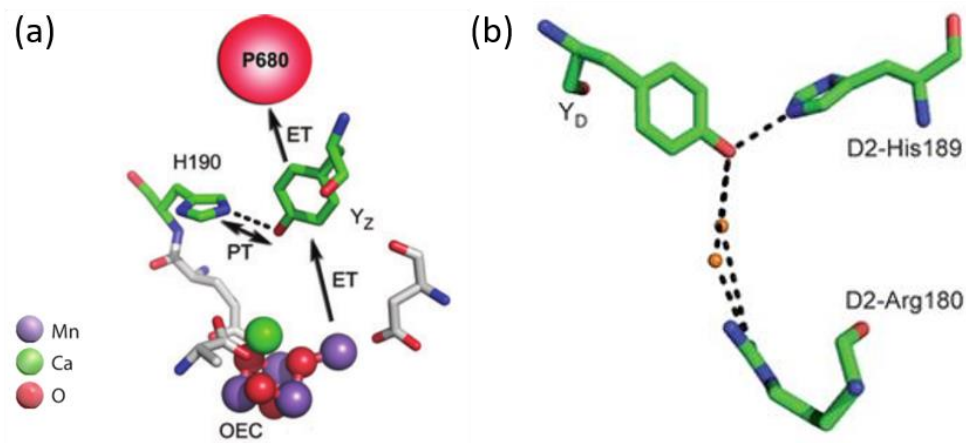

Figure1.1.1 Schematic diagram of the electron transfer pathway in photosystem II reaction center. (a) Tyr_z in the OEC of photosystem II. When the Tyr_z transfer electrons from the Mn_4Ca cluster catalyst in OEC to P_{680}, the proton transfer is accompanied by deprotonation of phenol in tyrosine to a histidine having imidazole functional group working as proton acceptor. Reproduced with permission.[1] Copyright 2009, Annual Reviews. (b) Another tyrosine, Tyr_D, which exist in photosystem II. In contrast to Tyr_z, it is relatively not surrounded by a hydrophobic domain. It does not work in water oxidation process and its true function is not fully known. Reproduced with permission.[2] Copyright 2015, Elesvier.

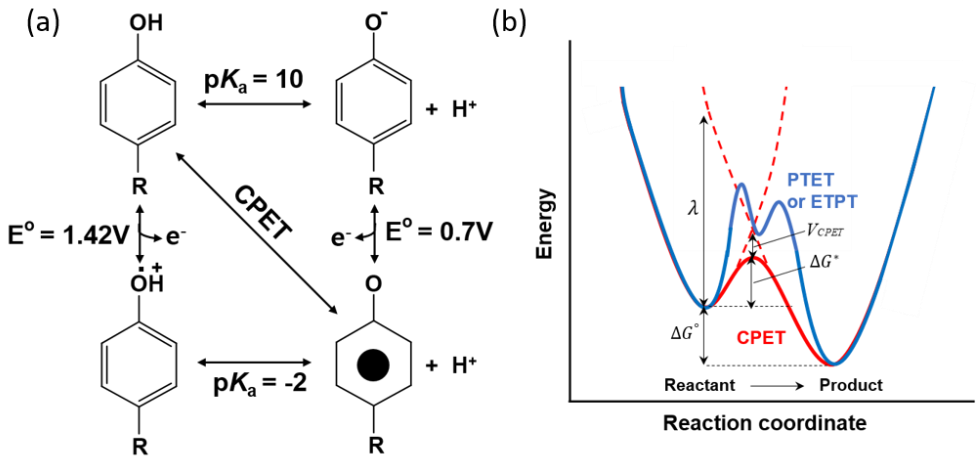

Figure 1.1.2 PCET of tyrosine. (a) Thermodynamic cycle of PCET for tyrosine radical formation. The diagonal pathway shows CPET mechanism while vertical and horizontal pathways show stepwise ETPT and PTET mechanisms. The CPET pathway avoids charged intermediates, effective in low dielectric media such as interior of proteins. Reproduced with permission.[3] Copyright 2018, John Wiley & Sons, Inc.

1.1.2 Model Studies for PCET of tyrosine

The mechanistic insights into PCET process can be a powerful tool for designing highly efficient water splitting catalysts or artificial photosynthesis for solar fuel generation. However, the mechanistic details of how electrons and protons are coupled are unresolved as it is not easy to study PCET of tyrosine in nature. This is because tyrosine containing system which in charge of PCET processes are complex and large biological systems. Thus, diverse biomimetic models with carefully controlled hydrogen bonding geometry have been investigated to define the PCET reaction mechanisms.[1,4,18–20]

The most commonly known model for discovering the effect of the protein environment on the tyrosine radical decay rate is the β-hairpin maquette (or peptide A), shown in Figure 1.1.3 (a). It is a designed 18-mer peptide inspired from photosystem II. The backbone sequence and the peptide folding induces the π-π stacking of tyrosine and histidine and indirect hydrogen bonding with water molecules. Similar to what occurs in photosystem II, a fast orthogonal PCET can be found in the decay of tyrosine radical. The rate of the PCET in peptide A is much faster than that of molecular tyrosine itself whose proton acceptor is surrounding water, suggesting an increased electronic and protonic coupling of tyrosine and proton acceptor histidine in peptide A as a result of non-covalent interactions induced by peptide folding.[4]

Another biomimetic platform to study PCET uses a tyrosine-photosensitizer complex, a complex which is a tyrosine-based phenol linked to a photosensitizer, normally $Ru(bpy)_3^{2+}$. When these complexes are irradiated by 460nm of visible light, the metal-to-ligand charge-transfer occurs, forming excited Ru^{2+} and subsequently oxidized into Ru^{3+} intermediate. As Ru^{3+} has high reduction potential (1.26 V vs. NHE), tyrosine can be oxidized and form radicals through PCET process. This simple platform has been widely used to investigate the rate dependence of the reactions on hydrogen bonding nature which can be affected by variables such as intramolecular/intermolecular proton-transfer distance using a different nearby bases or using different tyrosine-based phenol with an internal carboxylate base.

Studies on biomimetic model study for PCET converge to a conclusion that strong hydrogen bonding and shorter proton transfer distance promote the PCET, thus it can be dramatically changed by small geometric differences of hydrogen bonding.[21,22]

1.1.3 Artificial Photosynthesis Inspired by Tyrosine

PCET is a principle that can play a critical role in bridging the time scale of short living reactive intermediates formed by photo-induced charge separation to that of the relatively slow electron catalysis. Constructing artificial photosynthesis, stimulated by the PCET of tyrosine in photosystem II reaction center which shows the high quantum yield for water oxidation got attention as a roadmap to develop new platforms in the field of catalysis including water oxidation catalyst. Thus, numbers of biomimetic model were analyzed with long term goal of forming an experimental and theoretical platform for PCET process. The challenging step of designing artificial photosynthesis is mimicking intricate protein and radial interactions that can allow the generation of highly energetic but long-lived radicals. For a deeper understanding of complex natural system, lot of efforts are ongoing to practically apply the lessons from the tyrosine PCET process to build artificial photosynthesis systems for energy conversion equipment such as solar fuel cells and electrochemical devices.[9,12] Figure 1.1.3 (b) shows one example of artificial photosynthesis reaction center with high quantum yield for electron transfer from a water oxidizing catalyst to an oxidized dye, the triad-1 having benzimidazole-phenol porphyrin moieties (BiP-PF_{10}) attached to a nanoparticle such as SnO_2 or TiO_2. Upon irradiation with 532nm laser, an electron transfer occurs from excited porphyrin to nanoparticle and a second electron transfer which is coupled to an associated proton

transfer occurs from the phenol moiety of BiP to the porphyrin radical cation which is competent to P_{680}^{+}. The integration of BiP and a neutral phenoxyl radical formation in this system significantly improves the quantum yield of electron transfer to nanoparticles by rapidly reducing P_{680}^{+} and mitigating charge recombination reactions.[22,23] Recent efforts and advances on developing artificial photosynthesis reaction centers stimulated by tyrosine's role in nature may guide more efficient catalyst design for energy production in the future.

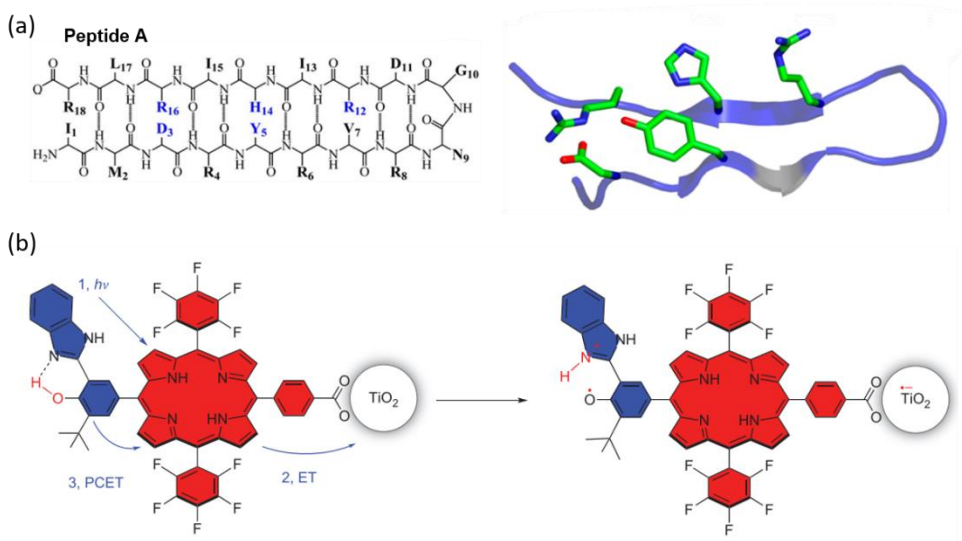

Figure 1.1.3 Biomimetic model system utilizing PCET. (a) Structure of a β-hairpin maquette *peptide A* : Backbone sequence and peptide folding induces π -π stacking of tyrosine and histidine and indirect hydrogen bonding with water molecules. Reproduced with permission.[4] Copyright 2015, American Chemical Society. (b) Artificial photosynthetic center *triad-1*. Upon irradiation (1), the system undergoes primary electron transfer (2) and a PCET reaction (3). Reproduced with permission.[5] Copyright 2014, Nature Publishing Group.

1.2 Studies to utilize Tyrosine's redox property : Tyrosine-rich short peptides YYACAYY

1.2.1 Tyrosine-rich peptide/MnOx hybrid material

Stimulated by the tyrosine-containing proteins in nature which are in charge of facilitating the concomitant transport of electrons and protons by tyrosine's redox activity, our group started to study diverse short peptide sequences containing tyrosine. Among various peptide sequences, YYACAYY (Y: tyrosine, A: alanine, C: cysteine) was deeply studied to explore the possibility of utilizing the tyrosine's unique redox activity in the future generation bioelectronics such as protonic devices or implantable electrodes.[6,24–26] It is known that when tyrosine is oxidized, it can be polymerized and form a molecule such as eumelanin which is a ubiquitous natural pigment having humidity-dependent electrical current and high proton conductivity, having high potential in utilizing in the future bioelectronic devices.[27–29] Taking this outstanding property into account, our group developed a facile strategy to oxidize the short 7-mer tyrosine-rich peptide by a powerful oxidant $KMnO_4$, aiming to form dityrosine cross-linking network. Peptide films were fabricated by spin-coating method and they were oxidized by immersing into $KMnO_4$ aqueous solution. As a result, simultaneous cross-linking of tyrosine and the hybridization of hydrophilic

manganese oxide embedded in the peptide film with the size of 4 - 12nm were formed. The films having the thickness of nearly 120 ± 15nm were characterized with various methods in Figure 1.2.1 such as Atomic Force Microscopy (AFM) to observe the surface microstructure, photoluminescence (PL) to confirm the formation of dityrosine and Mn 2p X-ray photoelectron spectroscopy (XPS) to identify the Mn valence states dominant with Mn^{2+} and Mn^{3+}. Our group confirmed the formation and incorporation of MnO_x in both the interior and the surface of the peptide film, indicating that water and ions can easily diffuse into the inner structure of the film and resulting in high proton conductivity. The most noticeable property of this peptide/manganese oxide hybrid film was observed with electrochemical impedance spectroscopy (EIS). EIS measures conductivities of the materials precisely using two-electrode configuration. Altering current (AC) was applied and a 'semicircle and tail' which is a typical shape of proton conductors contacted by an ion blocking electrode was observed. The hybrid film exhibited the high conductivity reaching maximum of 18.6 mS/cm at 90% RH at room temperature. This conductivity value is considerably high compared to other values reported from proton conducting materials such as eumelanin, serum albumin or reflectin protein from cephalopod, having 0.1 to 1mS/cm.[27,30–32] It was found out that both tyrosine-rich peptide sequence and MnO_x contributes to this high conductivity and humidity dependency. The kinetic isotope effect (KIE), the conductivity of the hybrid film in H_2O atmosphere over that in the presence of deuterium oxide (D_2O) vapor where

deuterium substitutes proton was also calculated by EIS measurement and the value was about 3.3, showing that the main charge carrier of the hybrid film are protons from water vapor. The KIE value is also high compared to proton conductors working at room temperature.[6]

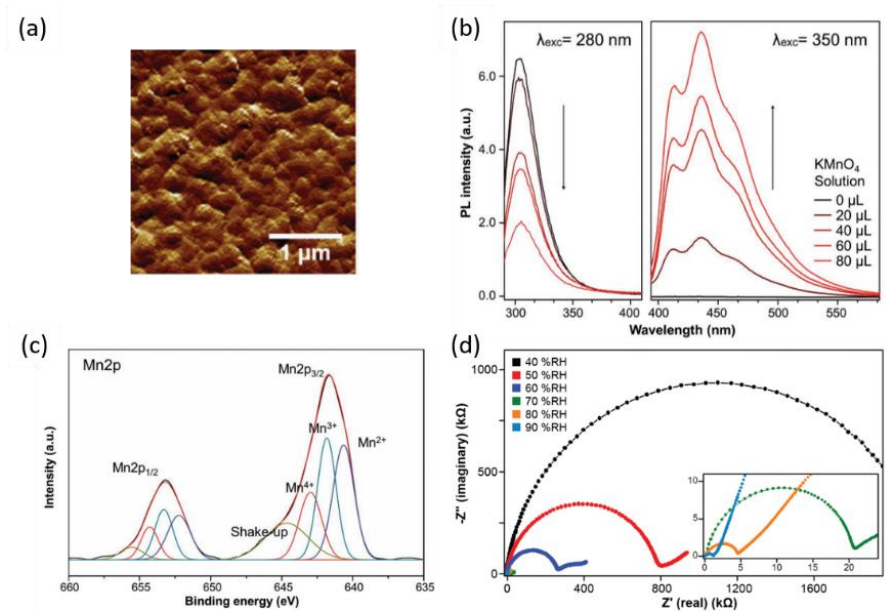

Figure 1.2.1 YYACAYY/MnOx hybrid film. The characteristics and unique properties were analyzed by various methods. (a) AFM image of the hybrid film showing a rough surface of the hybrid film. (b) The clear dityrosine formation was observed by photoluminescence spectrum. From the 280nm excitation and the resultant emission at 305nm which is the characteristic of tyrosine, its intensity decreased by increasing $KMnO_4$ treatment concentration. From 350nm excitation and the resulting emission at 410-415nm, the characteristic of dityrosine showed the formation of an extended conjugate system by dityrosine with increasing $KMnO_4$ treatment concentration. (c) Mn 2p XPS spectrum, showing the high valence Mn^{7+} reduction into reduced species in the hybrid film, dominantly Mn^{2+} and Mn^{3+}. (d) Nyquist plots measured from gold electrode two-terminal hybrid film device by impedance spectroscopy depending on the relative humidity. The semicircle and the inclined tail is a typical shape of proton conductors which in contact with ion blocking electrodes. The dependency on the relative humidity indicates the main charge carrier of the hybrid film is proton from water vapor. Reproduced with permission.[6] Copyright 2017, John Wiley & Sons, Inc.

1.2.2 Kinetic Isotope Effect for proton conduction study

A different reaction rate caused by an isotopic substitution is called kinetic isotope effect (KIE). This value arises as heavier isotope has a lower mobility and increased stability from the higher dissociation energies compared to lighter isotope. The KIE value is defined as the ratio of the reaction rate with the lighter isotope versus the reaction rate with the heavier isotope. For hydrogen and deuterium, the KIE is defined as :

$$KIE = \frac{k_H}{k_D}$$

There are two mechanisms responsible for proton conduction mechanism ; vehicle mechanism where proton migrate through the medium along with proton solvent such as H_3O^+ and $H_5O_2^+$ and Grotthuss mechanism, explaining proton conduction by proton hopping between neighboring charged and hydrophilic residues forming well aligned hydrogen bonding network. Theoretically, the KIE value for vehicle mechanism where proton transport only occurs by hydronium ion diffusion is strongly dependent on the vehicle diffusion rate so that the value equals the viscosity ratio which is approximately 1.2. The value for the Grotthuss mechanism where proton transfer occurs with the formation and breaking of hydrogen bonds, is about $\sqrt{2}$ as the attempt frequency to overcome the energy

barrier of hopping is related to the effective mass of the atom.[20,31] None of these two theoretical proton conduction mechanism KIE value matches with the KIE of the hybrid film and can't explain the mechanism of the peptide/manganese oxide hybrid film. The origin of the high KIE value of the peptide/manganese oxide hybrid film is still unknown, but it can be hinted from the tyrosine's major role in nature, the PCET process. KIE values of PCET cover a wide range as KIE for PCET reactions is approximately proportional to the square of the ratio of the reactant and product vibrational overlap for hydrogen to the overlap for deuterium which differ in a large range.[6,20,33,34]

The KIE value can be estimated from the ratio of conductivity measurements. To get KIE value of the hybrid film in our group, the conductivity measured from the EIS measurement with H_2O and D_2O vapor conditions were used and other studies such as study on gramicidin A ion channels, also used this calculation method.[6,35] A method to get KIE value by the definition is a transient absorption spectroscopy study. For example, the KIE value of PCET of the phenol-pyrrolidino fullerene was obtained. In this complex, the phenol hydroxyl group is hydrogen bonded to the lone pair electrons of the nitrogen on the pyrrolidine on the fullerene. This internal hydrogen bonding provides a well-defined structural framework for the CPET process. When the complex is excited at 705nm which is the lowest energy absorption band of fullerene, it becomes singlet excited state, subsequently becomes triplet state by PCET. The lifetime of the singlet state

becomes much shorter when there exists hydrogen bonding between phenol and pyrrolidine compared to non-hydrogen bonded fullerene complexes by hydrogen bonding modifications. By the transient absorption spectroscopy in H_2O and D_2O environment, the lifetime for decay of the phenol-pyrrolidino fullerene complex was measured and by estimating the rate of PCET, its KIE value was calculated as 3.0 and much higher for the weaker hydrogen bonding complexes.[36]

1.2.3 Tyrosine-rich peptide/MnOx hybrid nanofilm as a promising new material for electrical devices

Proton conduction is a ubiquitous phenomenon in nature which attracted increasing interest of materials scientists as the current of protons or other ions are more appropriate language than electrons in nature and involved in lots of electrical signaling pathways of living organisms. Prominent examples include ATP oxidative phosphorylation in mitochondria and proton channel of influenza M2 protein consists of histidine and tryptophan for virus replication.[37,38] In nature, as mentioned above, proton conduction is normally achieved by PCET, proton conduction which is coupled to the electron conduction. The development of modern electrical devices have been mainly focusing on controlling electronic currents. However, when considering the highly efficient signaling pathway in nature, not only electron conduction but also proton conduction that is coupled to the electron transfer may be a key for the next generation of electronics. Also, the nanostructured biocompatible solid state devices with biocompatible proton conductors may open a new opportunities for interfacing with living organisms, for example, the application in the biomedical field. Thus, interfacing the modern energy devices and biological proton conducting channels which have quite opposite characteristics and controlling the biological energy conversion, the proton conductivity and enhanced functionalities of these proton conducting materials can be applied to various

bioelectronics technologies including batteries, sensors, memristors, synaptic transistors and nanofluidics.[31,39]

Not only diverse proton conductors such as polymeric membrane Nafion, metal-organic frameworks, ceramic oxides, solid acids or naturally occurring proteins, but also the hybrid composite materials such as proton conductive proteins-carbon nanotubes composite have high potentials on giving multi-functionality over proton conduction.[27,30,31,39–44] These kinds of hybrid materials have advantages in enhancing water absorption, proton conductivity, mechanical and chemical stability by the incorporation of hydrophilic inorganic oxides or acids into an organic matrix. In this aspect, especially, the peptide/manganese oxide hybrid thin film which our group has developed is a good candidate for utilizing in device applications. Prior to the practically utilization of this high potential tyrosine-rich peptide/manganese oxide hybrid film in electrical devices and carry out high performances, the studies on mechanism of charge transport for the comprehensive knowledge of charge transport mechanism should be proceeded.

1.3 Mixed Ion-Electron Conductors as a model system to study and quantify PCET process

1.3.1 Mixed Ion-Electron Conductors

Inorganic materials having conduction mechanism similar to the PCET process is a mixed ion-electron conductor (MIEC) having a significant conduction ionically and electronically. The definition of MIEC often extends its meaning to include the materials that can conduct not only electrons and/or holes but also atoms in the materials. The most representative example of MIECs is oxide-ion and electron conducting oxide such as $BaTiO_3$ and CeO_2. Other commonly known MIECs are also shown in the Table 1.3.1. They include another type of oxides which conduct cations and electrons such as CoO and $LiMn_2O_4$, metals like palladium which can conduct protons and electrons after the hydrogenation and even include heterogeneously connected materials like Ni-YSZ (Y_2O_3-doped ZrO_2) cermets which can conduct holes (or electrons) and oxide ions (or oxygen vacancies), respectively.[7,45–49]

In the past, the law of independent migration, describing that different types of charge carriers migrate independently to each other, has been widely accepted as electron and ion interference effect has been usually ignored in the treatment of the

MIECs. This assumption is fulfilled in MIECs such as Ag_2Se and Cu_2S.[49] However, it turns out that it is not always the case. As recently been studied in various oxides such as $Fe_{3-\delta}O_4$, $TiO_{2-\delta}$ and $CeO_{2-\delta}$, a flow of ionic carriers inside the material can be induced indirectly by the electronic driving force even in the absence of the ionic driving force and vice versa for electronic flow of the sample. The interference effect is by no means negligible depending on their thermodynamic state such as temperature or the deviation from the stoichiometric composition.[7,8,45,50–56] Therefore, one has to take the cross effect or the non-zero cross coefficients into account when describing the transport equation of charge carriers.

MIEC	Charge carriers
$BaTiO_{3-\delta}$	O^{2-}, h^{+}
$CeO_{2-\delta}$	O^{2-}, h^{+}
$Co_{1-\delta}O$	Co^{2+}, e^{-}
$Li_xMn_2O_4$	Li^{+}, e^{-}
Pd	e^{-}, H^{+}
Ni-YSZ	O^{2-}, h^{+}

Table 1.3.1 Representative Mixed Ion Electron Conductors including various oxides working at high temperature, one element like palladium or even heterogeneously connected ionic and electronic conductors. The charge carriers having positive and negative charges vary widely with the type of materials

1.3.2 Transport equations and Onsager coefficients

According to the linear transport theory, in a mixed conductor, the cross terms, referred to as Onsager coefficients of transport, arise when more than one kind of mobile particle exists in the sample. As mentioned before, the ionic and electronic flows may interfere each other, i.e. flow of mobile anions or cations can cause an electronic flow while the flow of electrons can cause an ionic flow inside the sample. The generalized transport equations and derived transport parameters are summarized in Table 1.3.2.[57] In the table, transport equations relating fluxes and driving forces of carriers (the electrochemical potential η_e and η_i) are described with Onsager coefficients. The Onsager coefficients L_{ie} and L_{ei} values are equal according to Onsager reciprocal relations. In the transport equations, the partial current densities J_k (or i_k) and the electrochemical potential gradients $\nabla \eta_k$ are all experimentally measurable and controllable. Therefore, the four Onsager coefficients may be determined by these experimental technique ; (i) blocking ionic flow $\left(i_i = 0\ ;\ i = i_e\right)$ which provides transport parameters α_i^* and σ_e' (ii) blocking electronic flow $\left(i_e = 0\ ;\ i = i_i\right)$ providing transport parameters α_e^* and σ_i' which will be explained below.

First, as a measure of the interference effect, two parameters derived from Onsager coefficients were defined ; α_i^* which is called the ionic charge of transport

and α_e^*, the charge of transport of electron. As definition shows, they are the ratio between L_{ie} and L_{ii} or L_{ei} (= L_{ie}) and L_{ee}, respectively. Phenomenologically, α_i^* corresponds to the number of electrons dragged by an ion, which is an oxygen vacancy in case of oxide MIEC, in the absence of the direct cause for an electronic flow ($\nabla \eta_e = 0$), and α_e^* is also described in the same manner, the number of ions dragged by a mobile electron in the absence of direct driving force for proton movement ($\nabla \eta_i = 0$). For example, if the value of α_i^* gets higher due to the change in measurement conditions or nonstoichiometry, the interference among electrons and ions gets stronger as the cross effect α_i^* reduces the net charge transferred by a mole of ion to $\left(z_i - \alpha_i^*\right)F$ where z_i is a formal charge of an ion. This also can be regarded as reducing the mobility of ions by a factor of $\left(1-\alpha_i^*/z_i\right)$ because of the relaxation of the surrounding charge cloud due to the association of electrons. The two charge of transport are subject to the constraint :

$$\alpha_i^* \cdot \alpha_e^* = \frac{L_{ie}^2}{L_{ii}L_{ee}} < 1 \quad (2)$$

Usually for oxide MIECs, α_e^* is close to 0 while α_i^* is much higher, for example in $TiO_{2-\delta}$ it is in the range of 0.7 to 1.6 over the oxygen activity range examined.[50] It is inferred that the cross effect is a consequence of the coulombic interaction among charged particles. Then, the interference effect have to be reciprocal, but when

considering the counter relaxation effect between the central charge and its charge cloud, both the charge of transports are predicted to be roughly inversely proportional to the mobility ratio of the carriers in the charge cloud to the central carrier.[7]

In a DC polarization technique, the ionic and electronic conductivities with suppressed transfer of electronic or ionic charge carriers (σ_i', σ_e') are measured at the steady state where a stationary gradient of the component chemical potential is established. They are different from the partial ionic and electronic conductivities which are defined as ; $\sigma_i \equiv t_i\sigma$, $\sigma_e \equiv t_e\sigma$ where t_i and t_e each refers to ionic and electronic transference number and σ refers to total conductivity in the presence of the interference effect, evaluated from the instantaneous jump of potential upon switching on the current. The difference becomes significant as the interference effect becomes non-negligible. Although oxide MIECs have both ions and electrons as charge carriers, normally the prevailing charge carrier is electrons. Thus, $\sigma_e' \approx \sigma_{total}$ is satisfied if the measurement of a DC polarization method has been performed properly.[8,52,55,57,58]

Terms/Equations	Definition
$J_i = -L_{ii}\nabla\ \eta_i - L_{ie}\nabla\ \eta_e$ $J_e = -L_{ei}\nabla\ \eta_i - L_{ee}\nabla\ \eta_e$	Transport equations relating fluxes J_k (k = i,e) and the driving force or the electrochemical potential gradient of the k-type carriers.
L_{AB}	Onsager coefficients relating the flux of A (J_A) and the electrochemical potential gradient of the carrier B ($^{\nabla}\eta_B$)
$\alpha_i^* \equiv \frac{L_{ie}}{L_{ii}} = -\left(\frac{\nabla\ \eta_i}{\nabla\ \eta_e}\right)_{i_i=0}$	The charge of transport of ions which phenomenologically corresponds to the number of electrons dragged by a mobile ion in the absence of the electronic driving force
$\alpha_e^* \equiv \frac{L_{ei}}{L_{ee}} = -\left(\frac{\nabla\ \eta_e}{\nabla\ \eta_i}\right)_{i_e=0}$	The charge of transport of electrons which phenomenologically corresponds to the number of electrons dragged by a mobile ion in the absence of the electronic driving force
$\sigma_e' = \left(\frac{iF}{\nabla\ \eta_e}\right)_{i_i=0} = F^2 L_{ee}(1-\alpha_i^*\alpha_e^*)$	The electronic conductivity with suppressed transfer of ions
$\sigma_i' = -\left(\frac{iz_iF}{\nabla\ \eta_i}\right)_{i_e=0} = z_i^2 F^2 L_{ee}(1-\alpha_i^*\alpha_e^*)$	The ionic conductivity with suppressed transfer of electrons

Table 1.3.2 Transport equations relating fluxes and the electrochemical potential gradients of carriers and the resultant transport parameters α_i^*, α_e^*, σ_e', and σ_i'. The coefficient relating the flux and the driving force is called Onsager coefficient. The transport parameters are defined using Onsager coefficients and by controlling the current or the potential at the electrodes, it is possible to get four transport parameters and consequently four Onsager coefficients.

1.3.3 Experimental setup to get Onsager coefficients

Recently, a variety of appropriate experiments in order to measure the Onsager coefficients for various oxide MIECs were conducted. In addition, Onsager reciprocal relations was proved experimentally in Yoo's group and co-workers.[7,45,50–56] Experimental setups to investigate the interference of charge carriers have the same principle, which is, having both electron blocking electrodes and material blocking electrodes. Based on the theoretical background in the section 1.3.2, the specimen where the cations are practically immobile so that charge carriers are doubly charged oxygen vacancies $V_O^{\bullet\bullet}$ with a formal charge of + 2 and electrons (or holes) with a formal charge of –1 (or + 1), the electrochemical blocking cell in Figure 1.3.1 was constructed into the symmetric configuration. In the figure, metal such as platinum in bold navy line were used as ionic current blocking electrodes while YSZ at the both ends of the cell were employed to block electrochemically the electronic current. When the current pass through the specimen only, through probe 2 and $2'$, flow of ions at the electrodes are blocked which is referred to as 'Ion Blocking Mode'. When the current flows between 1 and $1'$, through both specimen and YSZ, it is called the 'Electron Blocking Mode'. Novel feature of this symmetrical cell is that not only electrons' electrochemical potential difference is measured by metal probes, but also the ion electrochemical potential difference is directly measured by YSZ probes 4 and $4'$ due to the local equilibrium reaction. Two Pt

wires (3 , 3′) were inserted into the sample prior to sintering process and serve to probe the electrochemical potential of the electrons along the current flowing directions while two oxide ionic probes made by YSZ are placed directly opposite to the Pt wires and serve as probes to measure the difference in the electrochemical potential of the oxygen vacancies.

The electrochemical potential of electron ($\Delta\ \eta_e$) is determined by the inner probes 3 and 3′ :

$$V = \frac{1}{F}\left(\eta_e^3 - \eta_e^{3'}\right) \quad (3)$$

By the local ionization equilibrium : $V_O^{\bullet\bullet} + O + 2e^- \rightleftharpoons O_O^X$,

equation (4) is satisfied with the understanding that $\nabla \mu_{O_O^X} \approx 0$ for the regular structure element O_O^X .

$$\eta_i = \mu_{O_O^X} - \mu_O - 2\eta_e \ ; \ \nabla\ \eta_i = -\nabla\ \mu_O - 2\nabla\ \eta_e \quad (4)$$

and by using equation (4) the ionic electrochemical potential difference can be directly measured by the inner probes 4 and 4′ :

$$U = \frac{1}{F}\left(\eta_e^4 - \eta_e^{4'}\right) = \frac{1}{2F}\left(\eta_i^{4'} - \eta_i^4\right) \qquad (5)$$

The electrochemical potential gradient $\nabla \eta_e$ and $\nabla \eta_i$ can be calculated by dividing the distances between two measuring probes.

As mentioned, the four Onsager coefficients can be determined experimentally by blocking ionic or electronic flow. There are two methods to achieve the blocking ionic or electronic current : potentiostatic ion/electron blocking which apply current bias or galvanostatic ion/electron blocking conditions which apply voltage bias to the sample. In the MIECs studies, chemical polarization was carried out in a galvanostatic mode which is passing a constant current from Pt electrode 1 to $1'$ or 2 to $2'$ until the steady state was achieved. The open-circuit voltage (OCV) across both the ionic and electronic probes were monitored. In either mode of operation, the extent of chemical polarization across the specimen was kept as small as possible by flowing the possibly low current level to regard the Onsager coefficients as constant in the oxygen chemical potential difference $\Delta \mu_O$ induced.[7,50]

In either ion or electron blocking conditions of the cell, when the current is applied, chemical potentials of ions or electrons are progressively developed respectively, counteracting the electrical driving force for the transport of ions or electrons. At the steady state where the ionic or electronic current is completely blocked, U or V respectively should become zero in the absence of interference effect between ions and electrons as it is directly proportional to the direct driving force for ionic transport $\nabla \eta_i$ or $\nabla \eta_e$. On the other hand, if non-negligible interference

effect exists, non-zero finite value of U or V are developed since the direct driving force $\nabla \eta_i$ or $\nabla \eta_e$ now have to counterbalance the driving force as a consequence of the interference effect and consequently achieve blocking of the ionic and electronic current at steady state, respectively. The finite value different from zero of U (or V) is the direct evidence for the existence of non-zero value of Onsager coefficients L_{ie} by transport equations in the Table 1.3.2.

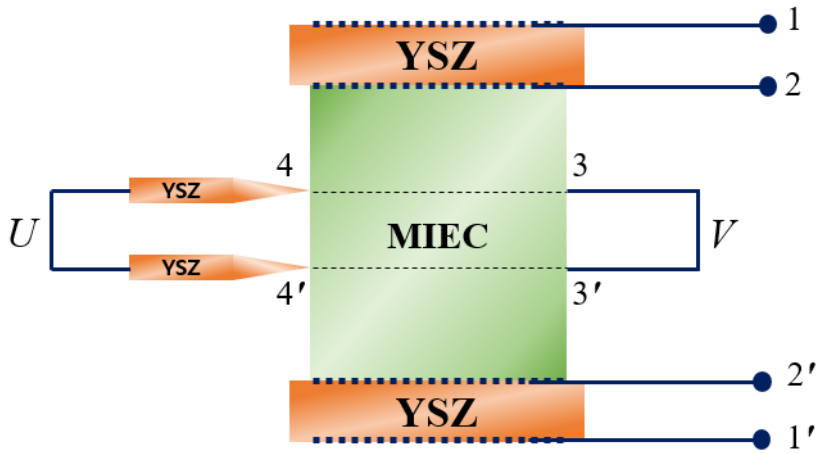

Figure 1.3.1 Common scheme of oxide MIECs sample to get four Onsager coefficients. Probes 1, 1′, 2, and 2′ are to give a fixed value of current to the sample while probes 3, 3′ and 4, 4′ are to measure the electrochemical potential of electrons and ions, respectively. Platinum electrodes are shown in dark navy line and porous Pt electrodes are shown in dark navy dashed line. For the oxide MIEC which conducts electrons and doubly charged oxygen vacancies, $V_O^{\bullet\bullet}$, Yttria Stabilized Zirconia(Y_2O_3-doped ZrO_2) is used as an electron blocking electrode which block the net electronic flow in the sample and measure the chemical potential of $V_O^{\bullet\bullet}$ at 4 and 4′ positions for both electron blocking and ion blocking mode. When flowing current through 1 and 1′, it becomes 'electron blocking mode' as YSZ at both ends of the specimen block electronic current to flow between 1 and 1′. When flowing current through 2 and 2′, it becomes 'ion blocking mode' as porous Pt blocks $V_O^{\bullet\bullet}$ movement at both ends of the sample.

1.3.4 Interference of charge carriers in inorganic materials

The direct indication of the interference of charge carriers can be found in the results of electrochemical potential measurement of MIECs, for example, $CeO_{2-\delta}$, shown in Figure 1.3.2. After the initiation of the current in either mode, a sharp increase is observed in the absolute values of U and V as predicted since the current is mixed ionic and electronic. It can be clearly seen that at the steady state, values of U and V are finite at O_2 atmospheric condition in Figure 1.3.2. As explained earlier, during ion or electron blocking operation and when the steady state is reached, the direct driving force for transport of ions U or electrons V, respectively, is required that will oppose the driving force due to interference, in order for the ionic or electronic current to be blocked. Also, the similar sign U and V at steady state in O_2 atmosphere is explained as a positive interference among the ionic and electronic flows, in other words, a flow of oxygen vacancies will tend to drag electrons in the same direction.[7,50] In case of MIEC $Ce_{0.8}Pr_{0.2}O_{2-\delta}$, the sample was also measured in CO/CO_2 mixture gas in order to impose very low oxygen activity. In contrast to the O_2 condition, the steady state values of U and V which are directly proportional to the direct driving force for ionic and electronic transport become almost zero, indicating that the interference effect is negligible in the CO/CO_2 mixture atmosphere case.[53] From the equations in the Table 1.3.2, the values of α_i^*, α_e^*, σ_e' and σ_i' can be determined and their dependency on oxygen activities which

determine oxygen nonstoichiometry or dependency on temperatures also can be discovered. For example for the MIEC $Co_{1-\delta}O$, the charge of transport of ions α_i^* was found to increase with increasing nonstoichiometry δ and with decreasing temperature.[45]

In fact, the cross term between electrons and ion fluxes is well known in the field of metals. Their interference becomes significant under high current density, known as electromigration which is a phenomenon that electrons pushing ions by momentum transfer regardless of the charge polarity of ions, resulting in the failure of metal contacts due to motion of the ions. However, in case of MIECs, there is no such electromigration and have no explanation on the interference effect except Onsager coefficients. The main reason why Onsager coefficients appear in describing transport equations in MIECs is because of an incomplete description of the system, meaning that there can be missing charge carriers we could not consider in advance. In oxide MIECs explained in the previous paragraph, we described the charge carriers as electrons and doubly charged oxygen vacancies, $V_O^{\bullet\bullet}$, however, another mobile ionic charge carrier, singly charged oxygen vacancies $V_O^{\bullet}$ may present in the MIECs. Therefore, if an appropriate defect model is considered and all three mobile species are included in describing the flux density equations, no cross terms are required. In the case of ceria, CeO_2, the meaning of Onsager coefficients can be explained like in Figure 1.3.3 by both singly and doubly charged oxygen vacancies and electrons. The metal electrodes in fact block material exchange, not

necessarily ion currents, in other words, it is only the net ion current which vanishes by the Pt blocking electrodes. This leads to a link between two oxygen vacancies fluxes under steady state conditions which have to be equal in magnitude and opposite in direction. Under an applied voltage in the ionic current blocking mode shown in Figure 1.3.3 (a), an electrochemical reaction (6) takes place at the interface between the MIEC and the anode :

$$V_O^{\bullet} \rightarrow V_O^{\bullet\bullet} + e^{-} \quad (6)$$

while at the cathode the inverse reaction to the electrochemical reaction (6) takes place. The consequence is that electrons are transferred by $V_O^{\bullet}$ from the cathode to the anode. Also, there exists an electronic current that flows through the oxide as it is a mixed conductor. The electrochemical reactions at the interface of the ceria and electrodes transfer the net ionic current within the ceria into an electron current within the metal electrodes. Similarly in the electron blocking mode in Figure 1.3.3 (b) when the electrodes block electron transfer and conduct $V_O^{\bullet\bullet}$ through them, at the anode side an electrochemical reaction inverse to (6) takes place with electrons which are generated by the electrochemical reaction (6) at the cathode side.[7,8]

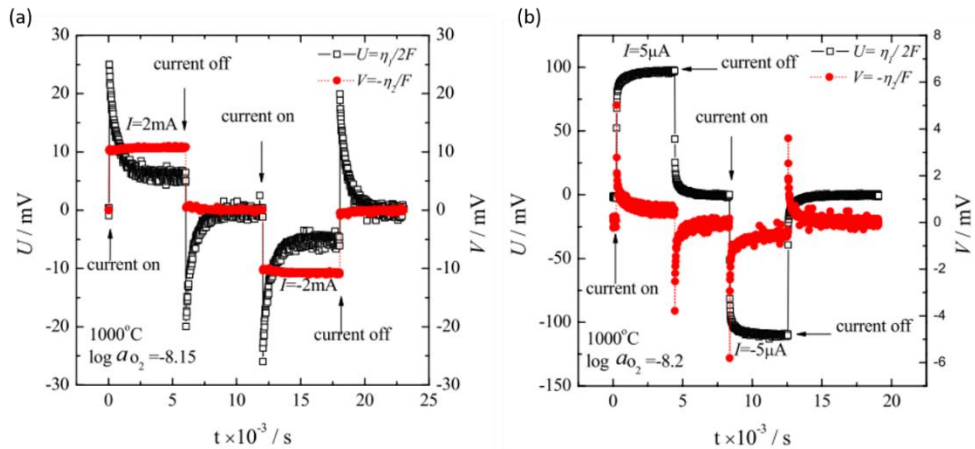

Figure 1.3.2 The responses of fabricated cell for CeO_2 conducting electrons and $V_O^{\bullet\bullet}$. (a) The figure shows the U and V vs. time in the ion blocking mode, indicating the ion and electron's electrochemical potential, respectively. When the current is on, U relaxes to a finite value which is not 0 while V almost immediately takes a steady state value. When the current is off, both U and V decay to zero and when the current passes in the opposite direction, it shows the same amount of variation with the first region (current > 0) but only in the opposite sign. (b) When a constant current flows in the electron blocking mode, the similar response to the U in the ion blocking mode is observed for V which relaxes to the non-zero finite value. Both results from (a) and (b) indicates the significant interference effect among ions and electrons. Reproduced with permission.[7] Copyright 2008, The Electrical Society.

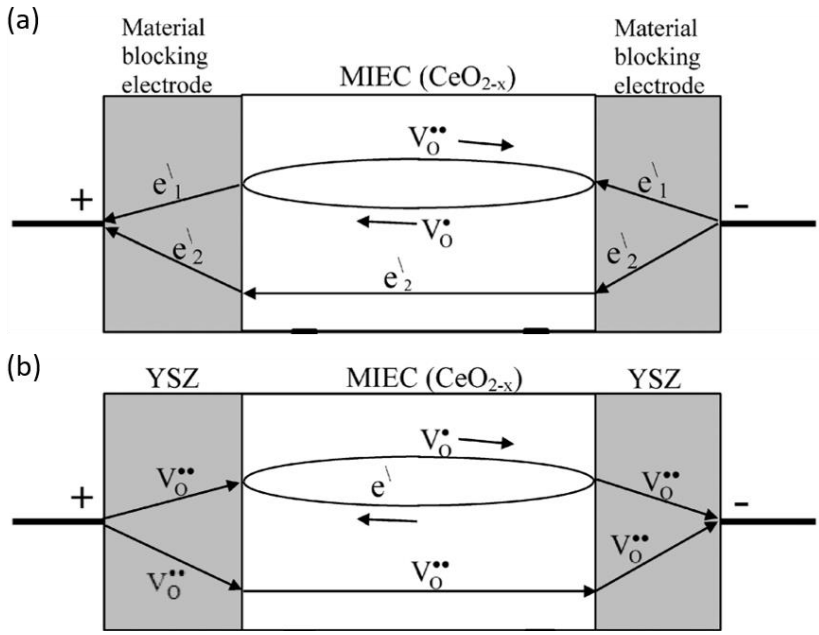

Figure 1.3.3 The fluxes in a MIEC conducting e^-, $V_O^{\bullet}$, $V_O^{\bullet\bullet}$. (a) When the electrode can conduct electrons and block material transfer through the electrode, electrochemical reactions at equilibrium take place in both anode and cathode. Under steady state, the net result is that electrons are transferred by doubly charged oxygen vacancies $V_O^{\bullet\bullet}$ from the cathode to the anode in addition to the electron current through the oxide. (b) When the electrode blocks electron transfer and conducts $V_O^{\bullet\bullet}$, electrochemical reaction takes place at the YSZ/MIEC interface . At the anode side, some of $V_O^{\bullet\bullet}$ defects are reduced to $V_O^{\bullet}$ while at the cathode side the inverse reaction occurs. The electron which reduces $V_O^{\bullet\bullet}$ into $V_O^{\bullet}$ are generated from the cathode which flow through the MIEC from the cathode to the anode. Reproduced with permission.[8] Copyright 2014, Royal Society of Chemistry.

Chapter 2. Study to quantify the PCET process of the Tyrosine-rich peptide/MnOx oxide hybrid film

2.1 Application of the concept 'Onsager coefficients' to the hybrid film's mechanistic study

As previously mentioned in Chapter 1, the mechanistic study of the proton conduction inside the tyrosine-rich peptide/manganese oxide film is crucial for future applications in devices connecting electronics and biological systems. The system contains complex, undefined network of hydrophilic manganese oxide nanoparticles and cross-linked peptides, having a limitation on detailed proton conduction mechanism study. Moreover, there has been no attempt to get direct parameter associated with proton and electron interactions by PCET reaction which may help in elucidating the conduction mechanism of materials quantitatively. MIECs in a large sense includes PCET which conducts protons and electrons simultaneously in one system, thus, the study on MIECs to get Onsager coefficients can be a good platform to study and quantify the transport parameters related to the PCET in various environment or film conditions. Therefore, in this context, we investigated the quantification of transport parameters of the tyrosine-rich

peptide/manganese oxide hybrid film which are related to the proton and electron interference due to PCET process. Although the dimension of the fabricated samples has been changed from three-dimensional to two-dimensional, the concepts of blocking one carrier at the electrodes while measuring electrochemical potentials of both carriers are maintained in our study.

In order to get all four Onsager coefficients and quantify the cross effect in detail, both protonic current blocking mode and electronic current blocking mode have to be conducted with the same sample at the same environmental conditions. As the tyrosine-rich peptide/manganese oxide hybrid material is prepared in the two-dimensional thin film, ion or electron blocking electrodes have to be placed over the hybrid film whereas three-dimensional MIECs sample have electrodes a the both ends of the specimen, make it possible for charge carriers to conduct inside the whole specimen. The three-dimensional MIECs setup can be used in both ionic and electronic blocking mode by using outermost YSZ and porous Pt pastes covering both ends of YSZ. However, in contrast to the MIECs setup, interior volume of the thin film inside the outer electrodes are considered as a part for charge carrier conduction. Thus, for the same volume used in ionic and electronic blocking mode system, two different samples with two different arrays of electrodes, which is outer proton blocking electrodes with inner electron blocking electrodes or outer electron blocking electrodes with inner ion blocking electrodes, should be prepared at once.[7,52]

Nafion membrane which is known for its high proton conductivity and its electron conduction blocking property has been considered as electronic blocking electrodes in our system.[41,59–62] However, to make electron blocking mode, the injection of protons through electron blocking electrodes is needed in addition to the electron blocking property. In order to inject protons into the hybrid film, materials such as palladium, which can conduct both protons and electrons, should be placed over the Nafion membrane. Then, by the electrochemical reaction on Pd (Equation (7)),

$$PdH_x \rightleftharpoons Pd + H^+ + e^- \quad (7)$$

protons and electrons are formed and only protons pass through Nafion, making complete electron blocking and proton injecting electrodes.[6] However, as three layers of rough materials meet each other forming two undefined interfaces, there are too many variables we have to consider such as interface resistance or the contact conditions which are thought to be possibly having bad effects on electrodes' functions to block electronic current and measure the electrochemical potential of protons. Thus, as a first trial of applying the concept of MIECs to the hybrid film for the identification and quantification of PCET process, we only proceeded proton blocking mode and investigated the regarding transport parameters.

2.2 Experimental Procedure

2.2.1 Chemicals

YYACAYY (tyr-tyr-ala-cys-ala-tyr-tyr, 98% purity) was purchased from GL Biochem (Shanghai, China) and used without further purification processes. 1,1,1,3,3,3-Hexafluoro-2-propanol (99% purity) and potassium permanganate (99% purity) were purchased from Acros organics and Sigma-Aldrich, respectively. Also, Nafion® N-115 membrane (0.125mm thickness, ≥0.90meg/g exchange capacity), purchased from Alfa Aesar was used after cleaning with a conventional method. It was boiled in H_2O_2 at 60℃ for 50 minutes to remove organic impurities, rinsed in boiling deionized water for 2 hours, boiled in 0.5M H_2SO_4 for 1 hour to remove any metal compounds and to replace Na^+ with H^+ in the membrane, and then rinsed in boiling deionized water for 2 hours. The Nafion membrane was stored in deionized water.

2.2.2 Peptide/MnOx hybrid nanofilm preparation

The hybridization of YYACAYY peptide film with manganese oxide using potassium permanganate solution was carried out by the tyrosine oxidation reaction.

A transparent 1wt% YYACAYY peptide solution in HFIP was prepared with heating at 50℃ for 30 minutes and with sonication to completely dissolve the peptide in the solution. A 50ul drop of solution was spin-coated on 1cm × 1cm cleaned SiO_2/Si substrate at the spin rate of 2000rpm with the holding time of 30 seconds. Annealing at 120℃ for 30 minutes was carried out to fully evaporate the residual solvent and it was immersed into a 30mM potassium permanganate solution with mild stirring of 100rpm, followed by washing with deionized water several times to remove remaining solution on the surface of the hybrid film. The thickness analysis was performed by using Alpha-Step D-500 which can provides thickness of the samples over 50nm. At least five points were analyzed to get the average value and the standard deviation of thickness.[6]

2.2.3 Proton blocking mode sample fabrication and the measurement

The proton blocking two-dimensional cell consists of two inner Nafion electrodes and two outer gold electrodes with the size of 1mm × 5mm and with 1mm spacing between electrodes. First, pre-treated Nafion® N-115 membrane was cut into 1mm × 5mm size and treated with air plasma for 40 seconds in order to make Nafion surface hydrophilic temporarily for the attachment on the hybrid film. This is because air plasma treatment can create peroxide and hydroperoxide on the

tetrafluoroethylene skeletons of the Nafion chain on the surface.[63–65] Two Nafion electrodes were then placed and pressed hard on the peptide/manganese oxide hybrid nanofilm with 1mm spacing. A pair of gold electrode with 70nm thickness were deposited by electron-beam evaporator onto the film through a shadow mask. The shadow mask was prepared with OHP film cut into a desired shape and size by the laser cutting method. The DC polarization experiment was conducted by Keithley 4200 semiconductor characterization system by applying a voltage (potentiostatic method) to gold electrodes while measuring a voltage between inner Nafion electrodes at room temperature at certain relative humidity (RH). The humidity was controlled by blowing humidified Ar gas with either H_2O or D_2O and it was monitored constantly during all electrical experiment using hygrometer. The transport parameters α_i^* and σ_e' were calculated from the same equations described in Table 1.3.2 :

$$\alpha_i^* = -\left(\frac{\nabla \eta_i}{\nabla \eta_e}\right)_{i_l=0}, \quad \sigma_e' = \left(\frac{iF}{\nabla \eta_e}\right)_{i_l=0} \qquad \text{(8-a, 8-b)}$$

Distance l inside the gold electrodes (5mm) were used for the thin film to calculate the gradient of η_e, $\nabla \eta_e$, and distance l' between the center of Nafion electrodes (2mm) were used to calculate $\nabla \eta_i$. :

$$\nabla \eta_e = \frac{-FV}{l}, \quad l = 5mm \quad ; \quad \nabla \eta_i = \frac{FU}{l'}, \quad l' = 2mm \qquad \text{(9-a, 9-b)}$$

2.3 Results and Discussions

2.3.1 Proton blocking mode of the hybrid film

The schematic diagram and the real image of fabricated proton blocking mode sample is shown in Figure2.3.1. We used potentiostatic measurement, applying a finite voltage to the sample, instead of galvanostatic measurement which flows a finite current to the sample. When the galvanostatic measurement is used, it is better to compare interference of protons and electrons of different kinds of samples or samples in different environment with the same amount of electron flow than potentiostatic measurement. However, practically, this is not a best choice, for instance, if humidity decreases the voltage needed to flow the same amount of current in the hybrid film increases dramatically so that the resultant high voltage might have a bad impact on Nafion state or Nafion's voltage to be overestimated. In contrast, the potentiostatic measurement makes it possible to compare interference effect and importantly excluding possible influences of outer gold voltages on inner Nafion electrodes. Also, the advantage of applying voltage instead of current is that we can easily compare the transport parameter α_i^* as one of the variables $\nabla \eta_e$ is fixed.

At first, the wide range of gold voltages were applied to the sample and the

resultant Nafion voltages were measured by metal probes on Nafion electrodes. A linear relation between gold and Nafion voltages can be found in Figure 2.3.2 and the error range of Nafion voltage with the deviation of the probe's position from the center of the Nafion was below 0.01V within one sample. According to the definition of the transport parameter α_i^*, the ratio of a Nafion voltage over a gold voltage is proportional to the cross effect of charge carriers if Nafion in practice measure the electrochemical potential of proton which will be discussed later. The linear relation observed from Nafion and gold voltages demonstrates that the amount of the interference among protons and electrons is almost constant regardless of voltages that we examined. Thus, among tested voltages, 0.6V has been taken as a voltage bias value to apply to the gold electrodes and induce mixed electronic and protonic current as it assures moderate current level and prevents the sample from undesired electrochemical reactions such as water electrolysis at near 1.5V.

We have taken the Nafion membrane, the state of the art proton conductor, as electron blocking electrodes which block electrons and measure the electrochemical potential of protons induced by PCET inside the hybrid film. The utilization of Nafion as electron blocking and proton electrochemical potential measuring electrodes is the fundamental argument of ours for the fabrication of the proton blocking mode sample. According to the water channel model commonly used to describe the conduction of ions in the Nafion, the sulfonic acid groups in Nafion organize into hydrophilic water channels through which small ions such as

protons can be easily transported whereas the conduction of electrons are blocked as water swollen Nafion gets negatively charged and block negatively charged species.[66,67] On the contrary to the well-known Nafion membrane's ability to block electrons, in our best knowledge there has been no attempts to attach Nafion membrane on a thin film sample for the measurement of the electrochemical potential of protons.

The logic of the argument on using Nafion for the measurement of proton electrochemical potential is summarized compared to the principle how YSZ can measure the electrochemical potential of the doubly charged oxygen vacancy $V_O^{\bullet\bullet}$ in Table 2.3.1. Definitely, in both cases the electrochemical potential of electrons of the sample is measured by metal probes directly on the sample or on metal electrodes. The principle of YSZ measuring the electrochemical potential of the $V_O^{\bullet\bullet}$ is based on the chemical reaction at equilibrium involving O^{2-} which can be considered as $V_O^{\bullet\bullet}$ reversely. Therefore, by the equation about U in Table 2.3.1, the voltage result from the measurement by YSZ, measuring U can be regarded as measuring $\Delta \eta_i$, the electrochemical potential of $V_O^{\bullet\bullet}$.[7,52] In the same manner, in our system which uses Nafion as the electrodes to measure the voltage induced by protons, the electrochemical potential can be measured by a chemical reaction at the Nafion electrodes at equilibrium with reference hydrogen gas in the atmosphere[68] :

$$\frac{1}{2}H_2 \rightleftharpoons H^+ + e^- \quad (10)$$

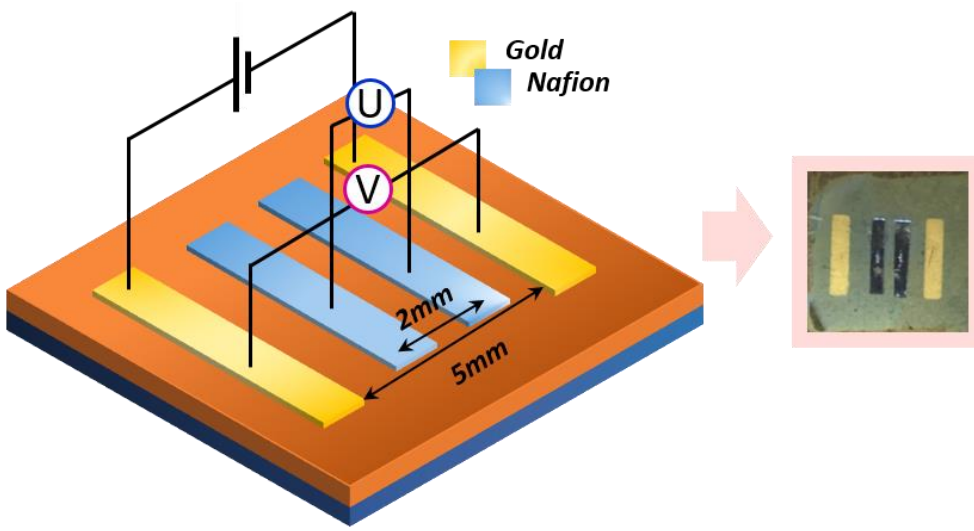

Figure 2.3.1 Schematic diagram and a real image of the sample fabricated into proton blocking mode system. Two gold electrodes are placed outer side while two Nafion membrane electrodes are placed inside with 1mm distance between electrodes. The proton blocking mode experiment was conducted by applying a fixed voltage on outer gold electrodes and measuring U from Nafion membranes and V from gold electrodes. The positions of all probes were kept close to the center of each electrode during the measurement.

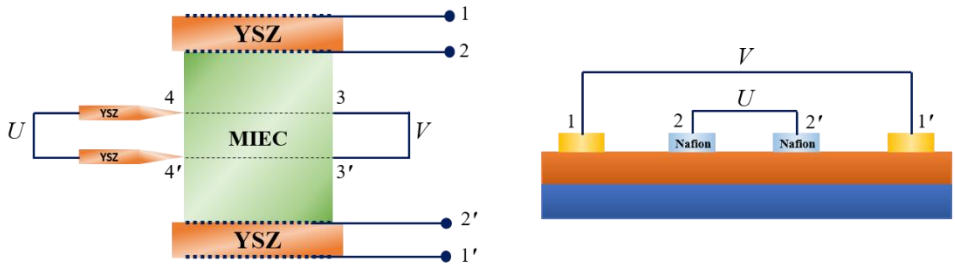

	YSZ	Nafion® N-115 membrane
Chemical reaction at equilibrium	$\frac{1}{2}O_2+2e^-\rightleftharpoons O^{2-}$ $\frac{1}{2}\mu_{O_2}+2\eta_{e^-}=\eta_{O^{2-}}$	$\frac{1}{2}H_2\rightleftharpoons H^++e^-$ $\frac{1}{2}\mu_{H_2}=\eta_{H^+}+\eta_{e^-}$
V	$V=\frac{1}{F}(\eta_e^3-\eta_e^{3'})$	$V=\frac{1}{F}(\eta_e^1-\eta_e^{1'})$
U	$U=\frac{1}{F}(\eta_e^4-\eta_e^{4'})=\frac{1}{2F}(\eta_i^{4'}-\eta_i^4)$	$U=\frac{1}{F}(\eta_e^2-\eta_e^{2'})=\frac{1}{F}(\eta_i^{2'}-\eta_i^2)$

Table 2.3.1 The principle on how each YSZ and Nafion electrode can measure the electrochemical potential of oxygen vacancies and proton. By the chemical reactions at equilibrium containing each O^{2-} (which can be considered as $V_O^{\bullet\bullet}$ with opposite sign) and proton, the voltage U measures the difference of electrochemical potential of oxygen vacancies and protons at specific positions.

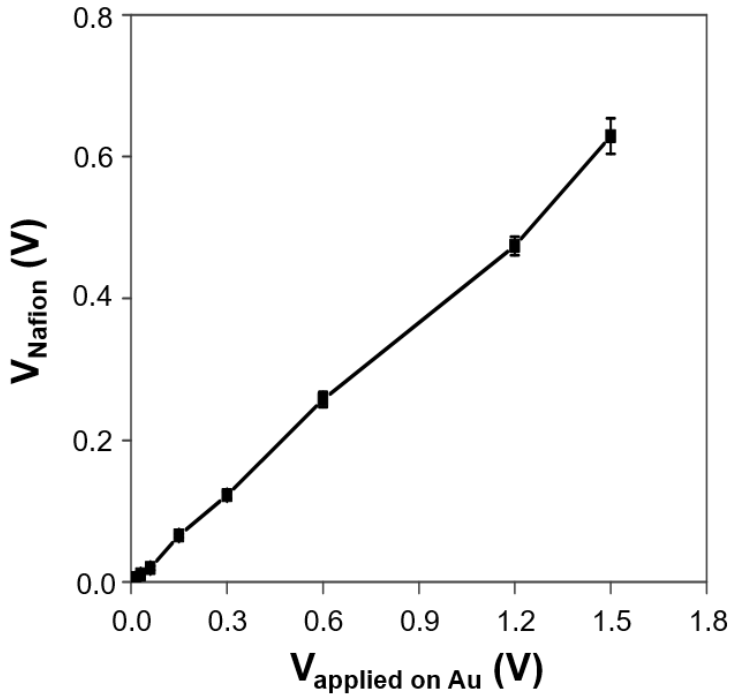

Figure 2.3.2 Nafion voltage according to the applied voltage on gold electrodes. The graph shows the linear relation between Nafion and gold voltages, indicating the interference among protons and electrons does not change regardless of applied voltage values.

2.3.2 Evidence of interference of protons and electrons

The investigation on the change of Nafion voltage was conducted by applying fixed voltage 0.6V, 0V, -0.6V and again 0V in a consecutive order to the outer gold electrodes for at least 5 minutes for each in order to reach the steady state. Figure 2.3.3 shows the resultant voltage measured at two different electrodes at the corresponding time and the corresponding applied voltage. In the figure, a region where the positive voltage was applied is colored in yellow whereas the region where negative voltage was applied is in orange. First, the proper working of the DC measurement of the hybrid film at 90% RH was confirmed by the current measured at the gold electrodes. The current successfully flew in the intended direction and saturated to the steady state value when the fixed DC voltage is applied to the sample and the same amount of current conducted inside the sample with the opposite direction when applying the voltage with the opposite sign. Most importantly analogous to the inorganic MIEC cases, the voltage U measured by Nafion membranes on the hybrid film representing the electrochemical potential of protons changed with the change of voltage bias. Also, the amount of change in voltage U is symmetric for the oppositely applied voltage with respect to the Nafion voltage in no voltage applying region. When applying no voltage (= 0V) to the sample, the voltage measured at Nafion electrodes showed an offset of ± 0.25 V. In our expectation, the value of Nafion voltage should be zero when there is no voltage

applied to gold contacts of the sample. However, the deviation is quite big, going against our expectation. The reason of the offset of signal U with no voltage bias is not clearly understood. For the moment, we assume that this unprecedented phenomenon is probably related to the negatively charged Nafion with the high humidity condition, possibly affecting the measurement of Nafion voltage.[67] In any case, the offset of Nafion voltage was found to remain approximately constant throughout a measurement and therefore it was taken as the uncertainty of the measurement. Figure 2.3.3 shows the result of one proton blocking mode sample having Nafion voltage almost 0V for 0V bias. In the figure, the measurement result of voltage U is shown, having a finite steady state value in the region where the finite gold voltage is applied. With the 0.6V voltage bias at 90% RH, the voltage U measured at Nafion membrane in the figure was 0.26 ± 0.01 V and when using different sample, the sample to sample variation was observed and having average value 0.22 ± 0.33 V when considering all results from other samples. The finite value is far from zero, demonstrating that the distinct interference among protons and electrons, which is considered to be the result of PCET, of the macroscopic film can be directly confirmed by the same method used in MIECs studies.

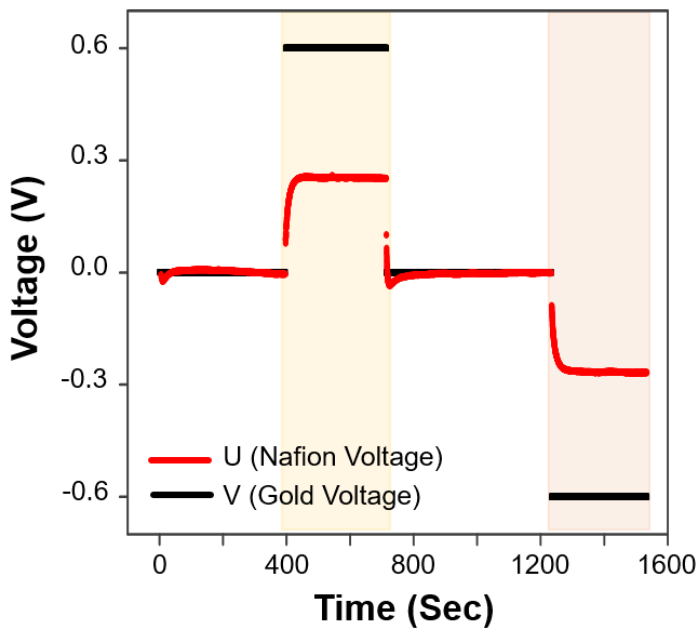

Figure 2.3.3 A result of fabricated proton blocking mode system of the hybrid film at 90% RH room temperature. The voltage applying regions are colored in yellow and orange, for each +0.6V and -0.6V. As clearly seen in the figure, the U measured from Nafion membranes on the hybrid film saturates to the finite value far from zero when applying gold voltages, indicating the significant interference effect of electrons and protons on their movement. The amount of change of voltage U is almost the same for oppositely applied voltage.

2.3.3 Hypothesis on proton electrochemical potential measurement of Nafion

2.3.3.1 Replacing Nafion electrodes with Gold

As far as we know, there has been no attempt to use Nafion as an electrode to measure the electrochemical potential of proton conducting inside proton conductors. Instead, there was an attempt to make a cell consisting of Nafion membrane and platinum electrodes fixed at both ends of the Nafion membrane. The cell was in contact with hydrogen and water vapor in order to get the transport number of water in this ionically conducting polymer Nafion. The cell potential was measured with platinum electrodes assumingly by the chemical reaction equation (10) at equilibrium.[68] However, it is still insufficient to claim that Nafion membrane connected to the metal probes of the equipment can read the electrochemical potential of protons of the material underneath the Nafion membrane.

One may dispute our argument that the voltage value measured by Nafion membrane can be interpreted as a proton's electrochemical potential between two positions. Also, it has been not confirmed whether the electrochemical potential of electrons at the positions under two Nafion electrodes which is developed by gold voltage bias influences the measurement of the accurate Nafion voltage. Therefore,

providing reasonable evidences on using Nafion membranes as true electron blocking and most importantly proton potential measuring electrodes which are not affected by electron at all are crucial for validating the rationality of our experimental system.

In order to present reasonable evidences of using Nafion membrane, in addition to the original proton blocking mode sample, we fabricated a modified sample having gold electrodes as inner electrodes instead of Nafion electrodes. The sample having four gold electrodes was made to compare the measured voltages from inner gold electrodes with voltages from inner Nafion electrodes to identify whether if the electrochemical potential of electrons developed inside the hybrid film affects the value of Nafion voltage. We expected if the electron electrochemical potential has a direct effect on Nafion, the trend of both gold and Nafion voltages may be the same with changing humidity conditions whereas there will be no similarities between voltages measured by gold and Nafion if the electrochemical potential of electron does not have an influence on Nafion. Thus, with these two samples measurement with applying fixed 0.6V to outer gold electrodes at various humidity conditions ranging from 40 to 90% were conducted. Prior to comparing the voltage from inner electrodes, the hybrid samples made in the same reactor having same reaction conditions that have fairly similar current made it possible for us to compare two different samples having different inner electrodes.

The voltages measured by inner gold electrodes have different values and

different tendency toward relative humidity when comparing the voltages measured by Nafion electrodes. As a result shown in Figure 2.3.4, the voltage from gold electrodes did not change according to the humidity variation. It has almost consistent value about 0.171 ± 0.002V while the voltage measured by Nafion in different humidity conditions has higher, almost the same value 0.235 ± 0.023V at 50 to 90% RH and drastically inclines with decreased humidity to 40% RH ($0.092 \pm$ 0.032V) which will be discussed further in the section 2.3.4. The result from inner gold electrodes may provide us an evidence to support the validity of using Nafion, which is, the voltage measured by Nafion which is considered to be having electron blocking and proton electrochemical potential measuring properties is not directly affected by the electron electrochemical potential developed by outer gold voltage bias at inner electrodes positions.

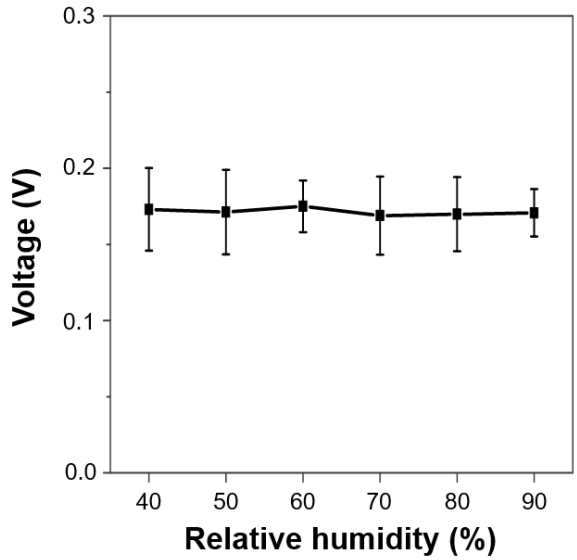

Figure 2.3.4 The voltages measured from inner electrodes when they are replaced with gold instead of Nafion. The experiment was held in order to confirm that Nafion voltage does not measure the electrochemical potential of electrons developed by the applied voltage at the outer gold electrodes. The measurement was conducted with samples having similar current level at various relative humidity ranging from 40 to 90% and the same voltage 0.6V was applied. As clearly shown in the figure, voltages from inner gold electrodes does not change according the relative humidity.

2.3.3.2 Nafion voltage on Non-proton conducting materials

Another experiment was considered to confirm that the electrochemical potential of electrons underneath the Nafion membrane does not have a strong influence on the measurement of Nafion voltages and to support our core argument that Nafion membranes can work as true electron blocking electrodes we seek. Samples with different kinds of film having no proton conduction were fabricated with maintaining the geometry and type of electrodes. The measurement of Nafion voltages were conducted in the same manner with the proton blocking mode and two widely studied materials were used as the specimen different from the hybrid film ; Indium gallium zinc oxide (IGZO, In_2O_3:Ga_2O_3:ZnO=1:1:1 mol%) deposited on SiO_2/Si substrate with the thickness of 50nm by the sputtering method and the bare Si wafer. The measurement was held in the moderate humidity 60% RH since it is known that for IGZO and Si, exposure to high humidity for a long time can change the electronic properties of the materials largely.[69,70] Also, there is a possibility of the formation of ultrathin water layer on the materials' surface when exposed to the high humidity for a long time and if the water layer gets thicker, it might affects the measurement of the Nafion voltage.[71] With the application of both ± 0.6V on gold electrodes, absolute current value of 5.09 ± 1.61 mA for Si wafer and the extremely low current for IGZO which cannot be detected by the measuring equipment were observed. The resultant Nafion voltages on both Si wafer and thin IGZO film are

shown in Figure 2.3.5. Regardless of the on/off of the voltage bias, it has been found out that Nafion voltage value at the steady state does not change. The results demonstrate that the voltage measured at Nafion membranes attached to the specimen is not affected by the gold voltage outside and does not show a change in voltage value if the underneath material has no significant proton conduction. As previously mentioned, it can be also seen that the saturated, the steady state voltage of Nafion have a finite value of about 0.3V for both IGZO and Si regardless of the applied voltage on gold electrodes. This finite value was maintained when the connection of probes 2 and 2′ in the table 2.3.1 to the measuring equipment was changed, implying that Nafion voltage which deviated from zero is not an equipment problem and probably factors in the sample are the cause of non-zero voltages. It can be simply due to the contaminated gold probes that measure the Nafion voltage or more seriously it can be due to different ion channel cluster distribution in two Nafion, making it two different electrical state. Also, the different interface between two Nafion and the hybrid film or even the different electrical state of Nafion and metal probe might affect the measurement of the Nafion voltage. However, it is not clear why voltages measured at the Nafion membrane are having specific values far from zero and further studies on Nafion/hybrid film interface or the Nafion itself should be conducted. At this moment, we are assuming the reason of this offset as two different Nafion states due to different ion channel cluster distribution, thus, planning to control the Nafion electrodes area and compare the result.

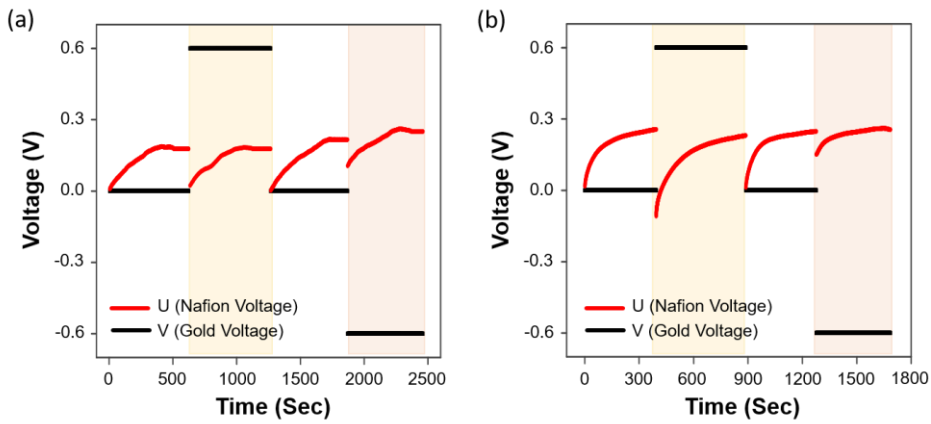

Figure 2.3.5 The responses of fabricated proton blocking mode at 60% RH using IGZO and Si wafer as non-proton conducting materials. (a) The Nafion voltage measured from the IGZO with changing the outer gold electrodes voltage in the order. There is no significant change in Nafion voltage with the change of gold voltages. (b) The Nafion voltage measured from the Si wafer. There is also no significant change found in Nafion voltage and the size of offset is similar to the IGZO case, implying that the origin of offset does not depend on the substrate.

2.3.4 Transport parameters of the hybrid film

2.3.4.1 Effect of Humidity on transport parameters

From the proton blocking mode measurement, the calculation of two transport parameters α_i^* and σ_e' were proceeded with the voltage value averaged with four different samples each of which measured more than three times at different probe positions around the center of gold and Nafion electrodes. Figure 2.3.6 shows the result of calculated α_i^*, the ratio between Onsager coefficients L_{ie} and L_{ii}, and σ_e' which is the electronic conductivity when proton transfer is blocked at the electrodes using equations (8) and (9). From the calculation using Nafion voltages over a wide range of humidity, as can be seen in Figure 2.3.6 (a), the value of α_i^* near 1 for the humidity range of 50 to 90% RH was observed while its value drastically decreases with low relative humidity (40% RH). The result clearly shows the fact that humidity of the environment affects the value of α_i^* calculated from Nafion voltages. According to the definition of α_i^*, phenomenologically it means that when there is no direct driving force of electron movement ($\nabla \eta_e$), one proton movement by $\nabla \eta_i$ can drags approximately one electron on its moving due to the interference effect. In inorganic cases, depending on the oxygen activity at 1000℃,

the α_i^* was in the range of 0.7 to 1.6 for CeO_2 with charge carriers $V_O^{\bullet\bullet}$ and e^- and 1.5 to 3.7 for TiO_2 with charge carriers Ti^{4+} and e^-.[7,50] In our case, we observed the value around 1 at wide humidity range at room temperature ; this is the first example of measuring and quantifying PCET in the bulk state. The σ_e' in Figure 2.3.6 (b) is decreasing with the decreasing humidity. The fact that σ_e' is affected by humidity can be easily predicted since the cross term α_i^* has the finite value much higher than zero, clearly confirming the PCET inside the hybrid film so that the electronic conductivity can be influenced by humidity which determine the proton motion. The value α_i^* decreases in large amount when the relative humidity reaches 40%. This is assumed as a result of bad hydrogen bonding condition inside the film which contributes largely to the proton and electron coupled conduction. Therefore, it can be anticipated that at the environment with low humidity, the value of σ_e' would not include the effect of the interference among protons and electrons, meaning that if it becomes vacuum state, probably the value of α_i^* would reaches zero and the σ_e' would become as purely electronic conductivity σ_e. Also, it can be expected that if the film is humidified with D_2O instead of H_2O, the value of transport parameters α_i^* and σ_e' both will have similar value at low humidity when compared to H_2O vapor environment and on the other hand, the values at high humidity can be largely different. Experiments using D_2O to investigate the isotope effect were indeed conducted at various humidity and they will be discussed in the

next section.

The error range of α_i^* at 40% RH is much higher compared to that at 90% RH. From the equation (8-a), the error range of α_i^* is determined by the error of the voltage measured by Nafion membrane electrodes. The high error of the voltage from the Nafion membrane measurement at low humidity condition may be resulted from the significant reduction of proton conductivity of Nafion membrane at low humidity. As the origin of high proton conductivity of Nafion membrane comes from the hydrophilic water channel which makes it easy to transport small ions, the proton conductivity of Nafion membrane gets much lower when placed in low humidity compared to that at high humidity condition.[41] We are assuming that the principle of the voltage measurement at the Nafion is the electrochemical reaction including a proton at equilibrium with ambient hydrogen gas in air (equation (10)). The time to reach equilibrium will be much longer and the equilibrium state might be much more unstable for low RH condition due to the unstable and not well-constructed water channel inside the film. Although the conductivity of Nafion membrane is reduced largely by the decreasing humidity, its conductivity value is about 1mS/cm at room temperature for anhydrous condition and it is still significantly high compared to the hybrid film having approximately 0.001mS/cm at vacuum condition. Therefore, it is thought that the voltage value measured by Nafion at 40% RH is still reliable for the proton blocking mode operation of the hybrid film.[72]

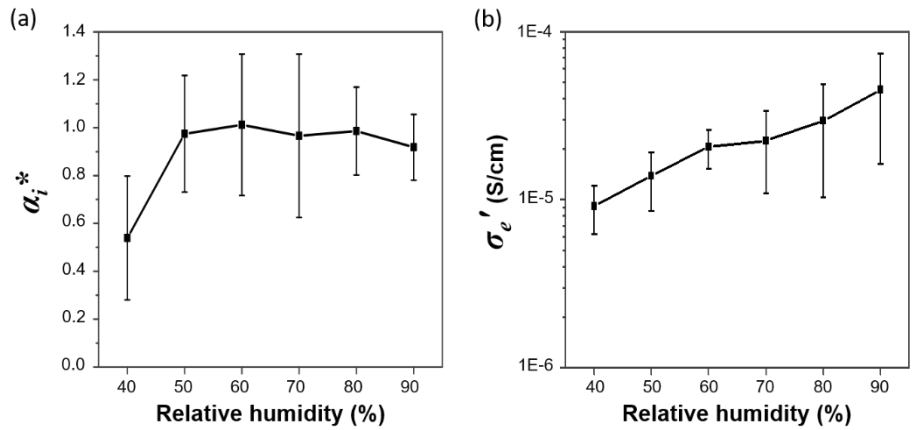

Figure 2.3.6 Transport parameters of the hybrid film at various humidity conditions ranging from 40 to 90% RH at room temperature. (a) The transport parameter α_i^* has a value approximately 1 at 50 to 90% RH while showing a low value near 0.5 at 40% RH. The observation of the value 1 indicates that one proton conduction is coupled to the one electron conduction, showing the proton-coupled electron transfer process in the macroscopic hybrid film. The decrease of the value implies PCET is not significant at low humidity assumingly due to the decreased hydrogen bonding network, which facilitate the PCET. (b) The transport parameter σ_e' increases with the increasing relative humidity. The result also demonstrates that protons modulated by humidity do affect the conduction of electrons, which is PCET.

2.3.4.2 Effect of Deuterium (Isotope effect)

The proton blocking measurement in the presence of D_2O vapor instead of H_2O was conducted to investigate the isotope effect on transport parameters. Figure 2.3.7 shows the calculated transport parameters results. Like in the H_2O-humidified film, film humidified with D_2O also has σ_e' values decreasing with the decreasing relative humidity and showing slightly lower values than that at H_2O environment. The difference between σ_e' values at H_2O and D_2O conditions are decreasing as humidity decreases. The decreased gap between σ_e' at 40% RH has already been predicted as α_i^* dramatically decreases to much lower value than 1 at 40% RH. This support our hypothesis in the last section that σ_e' would not affected by the interference among protons and electrons at low RH. The lower σ_e' with D_2O vapor compared to H_2O condition can be interpreted as the effect of the heavier mass of ion isotope coupled to the electron transfer. Since the electron and proton transfer are coupled together, the decreased mobility of ion due to the usage of heavier isotope will decrease the speed of coupled electron's conduction, thus, showing lower electronic conductivity value with D_2O-humidified air. This can be regarded as another evidence and experimental reproduction of PCET process of the hybrid film.

KIE, which provides us with the kinetic information of proton conductors

when deuterium replaces proton inside the film, was defined as the rate of hydrogen over that of deuterium. It was also given as the ratio of conductivity of proton over that of deuterium. Here, we define KIE in another way, by using the electronic conductivity with suppressed transfer of ions at the electrodes. As the electronic conductivity with suppressed transfer of either proton or deuterium at the electrodes contain the effect of each ion by PCET, we define KIE as the ratio of σ_e' at H_2O and D_2O humidified condition. According to this new definition, when the ion (proton or deuterium) transfer and the electron conduction interfere each other with the significant coupling i.e. the proton conductor whose conduction is governed by PCET process, the KIE value would have a value higher than 1 and the value would get higher if the coupling between ion and electron is much stronger. The kinetic isotope effect value calculated by the new definition of KIE in the hybrid film has a value of nearly 1.5 for 50 to 90% RH and 1 at 40% RH.

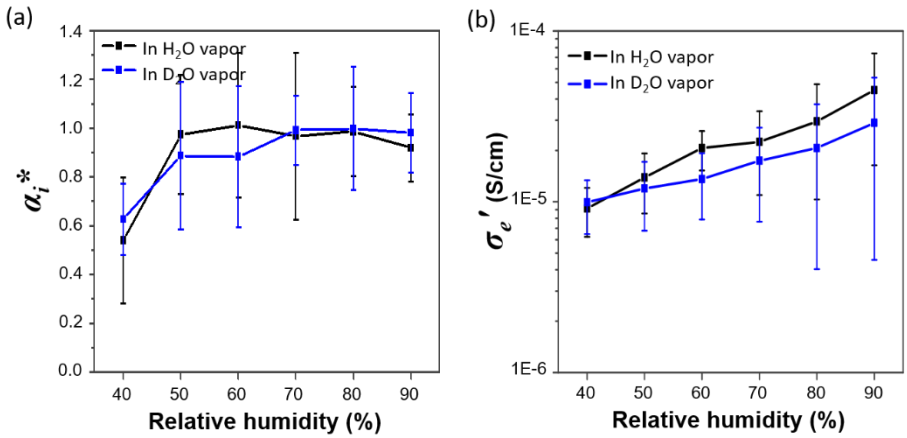

Figure 2.3.7 Transport parameters of samples humidified with H_2O(black line) and D_2O(blue line) vapor. (a) The transport parameter α_i^* of either operation has a similar value at the wide range of relative humidity. The result demonstrates that significant interference also exists between the conduction of deuterium and electron. (b) The transport parameter σ_e' of either condition is affected by relative humidity, decreasing with decreasing humidity. The electronic conductivity σ_e' with the film humidified with H_2O vapor is slightly higher than that of the film humidified with D_2O vapor. This can be interpreted as the effect of different ion mobility as a result of two times heavier mass of deuterium, affecting the conduction of surrounding electrons to be much slower.

Chapter 3. Conclusion

The measurement of proton electrochemical potential arising from the PCET process inside the proton conducting material is unprecedented. Before in diverse studies on elucidating the basic physical principles of the PCET, the kinetic isotope effects for a series of model PCET reactions were analyzed depending on the properties such as temperature, driving force and equilibrium proton donor-acceptor distance, consequently leading to large variation in KIE value. In this study, we proposed a new method for the PCET study which can be applied to various proton conducting materials in order to make it easy to confirm and elucidate bulk PCET mechanism by giving a quantified information about the effects of properties on PCET.

First, to the best of our knowledge, the Nafion membrane was first utilized as an electron blocking electrode which blocks electron movement and measures the electrochemical potential of protons. The sample for the operation of the proton blocking mode was fabricated in four electrode system ; using two proton blocking gold electrodes outside and two electron blocking Nafion membrane electrodes inside. Second, the measurement of Nafion voltage with different humidity and with different samples showed that the proton movement by PCET where net protonic current at outer electrodes is stopped can be directly measured by the voltage obtained from Nafion membrane electrodes. The calculation of transport parameters

analogous to the mixed ion-electron conductor studies was also conducted with the proton blocking mode operation of the tyrosine-rich peptide/manganese oxide hybrid film which has been discovered as highly proton conducting material working at low temperature. As a result, humidity dependency of σ_e' and α_i^* value close to 1 were confirmed, supporting the prevalence of PCET process in the hybrid film.

Although the trial to apply proton blocking mode operation was successful, it is still insufficient to get four Onsager coefficients and compare the interference effect among protons and electrons in different environmental conditions. Therefore, further study is required for the comprehensive knowledge of exact charge conduction mechanism.

In summary, we have presented a new approach to study PCET. Stimulated by the inorganic MIECs whose interference among charge carriers has been reported using transport parameters and Onsager coefficients for the convenience in interpreting the charge transport mechanism of complex MIECs, this study propose a method to apply the concept of transport parameters to the previously studied highly proton-conducting tyrosine-rich peptide/manganese oxide hybrid film. The change of Nafion voltage was observed with the change of voltage applied on proton blocking electrode, making net protonic current to be zero and counterbalancing the proton movement by PCET. We predict that the exploration of PCET of macroscopic materials with this simple operation may open a new chapter in the PCET study.

References

1. Reece, S. Y. & Nocera, D. G. Proton-Coupled Electron Transfer in Biology: Results from Synergistic Studies in Natural and Model Systems. *Annu. Rev. Biochem.* **78,** 673–699 (2009).

2. Barry, B. A. Reaction dynamics and proton coupled electron transfer: Studies of tyrosine-based charge transfer in natural and biomimetic systems. *Biochim. Biophys. Acta - Bioenerg.* **1847,** 46–54 (2015).

3. Lee, J., Ju, M., Cho, O. H., Kim, Y. & Nam, K. T. Tyrosine-Rich Peptides as a Platform for Assembly and Material Synthesis. *Adv. Sci.* **1801255,** 1–15 (2018).

4. Pagba, C. V., Chi, S. H., Perry, J. & Barry, B. A. Proton-coupled electron transfer in tyrosine and a β-hairpin maquette: Reaction dynamics on the picosecond time scale. *J. Phys. Chem. B* **119,** 2726–2736 (2015).

5. Megiatto, J. D. *et al.* A bioinspired redox relay that mimics radical interactions of the tyr-his pairs of photosystem2. *Nat. Chem.* **6,** 423–428 (2014).

6. Lee, J. *et al.* Proton Conduction in a Tyrosine-Rich Peptide / Manganese Oxide Hybrid Nanofilm. *Adv. Funct. Mater.* **27,** 1–9 (2017).

7. Park, W.-S., Yang, I. & Yoo, H.-I. Onsager Transport Coefficients of Mixed Ionic Electronic Conduction in CeO2-δ. *ECS Trans.* **13,** 327–336 (2008).

8. Riess, I. How to interpret Onsager cross terms in mixed ionic electronic conductors. *Phys. Chem. Chem. Phys.* **16,** 22513–22516 (2014).

9. Hammes-Schiffer, S. Theory of proton-coupled electron transfer in energy conversion processes. *Acc. Chem. Res.* **42,** 1881–1889 (2009).

10. Barry, B. A. Proton coupled electron transfer and redox active tyrosines in Photosystem II. *J. Photochem. Photobiol. B Biol.* **104,** 60–71 (2011).

11. Barry, B. A. *et al.* Proton Coupled Electron Transfer and Redox Active Tyrosines: Structure and Function of the Tyrosyl Radicals in Ribonucleotide Reductase and Photosystem II. *J Phys Chem Lett* **3,** 543–554 (2012).

12. Hammarström, L. & Styring, S. Proton-coupled electron transfer of tyrosines in Photosystem II and model systems for artificial photosynthesis: the role of a redox-active link between catalyst and photosensitizer. *Energy Environ. Sci.* **4,** 2379 (2011).

13. Sattler, M. & Valca, J. A Manganese/Iron Cofactor in Chlamydia trachomatis Ribonucleotide Reductase. *Science (80-.).* **316,** 1188–1191 (2007).

14. Minnihan, E. C., Nocera, D. G. & Stubbe, J. Reversible, Long-Range Radical Transfer in E. coli Class Ia Ribonucleotide Reductase. *Acc. Chem. Res.* **46,** 2524–2535 (2013).

15. Mathes, T. *et al.* Hydrogen bond switching among flavin and amino acids determines the nature of proton-coupled electron transfer in bluf photoreceptors. *J. Phys. Chem. Lett.* **3,** 203–208 (2012).

16. Mayer, J. M. & Rhile, I. J. Thermodynamics and kinetics of proton-coupled electron transfer: Stepwise vs. concerted pathways. *Biochim. Biophys. Acta - Bioenerg.* **1655,** 51–58 (2004).

17. Stubbe, J., Nocera, D. G., Yee, C. S. & Chang, M. C. Y. Radical Initiation in the Class I Ribonucleotide Reductase: Long Range Proton Coupled Electron Transfer? *Chem. Rev.* **103,** 2167–2201 (2003).

18. Lennox, J. C. & Dempsey, J. L. Influence of Proton Acceptors on the Proton-Coupled Electron Transfer Reaction Kinetics of a Ruthenium-Tyrosine Complex. *J. Phys. Chem. B* **121,** 10530–10542 (2017).

19. Muñoz-Rugeles, L. *et al.* Non-covalent π–π stacking interactions turn off non-adiabatic effects in proton-coupled electron transfer reactions. *Phys. Chem. Chem. Phys.* **78,** 1026–1037 (2017).

20. Hammes-Schiffer, S. & Iordanova, N. Theoretical studies of proton-coupled electron transfer reactions. *Biochim. Biophys. Acta* **1655,** 29–36 (2004).

21. Zhang, M. T., Irebo, T., Johansson, O. & Hammarström, L. Proton-coupled electron transfer from tyrosine: A strong rate dependence on intramolecular proton transfer distance. *J. Am. Chem. Soc.* **133,** 13224–13227 (2011).

22. Irebo, T., Johansson, O. & Hammarström, L. The rate ladder of proton-coupled tyrosine oxidation in water: A systematic dependence on hydrogen bonds and protonation state. *J. Am. Chem. Soc.* **130,** 9194–9195 (2008).

23. Mora, S. J. *et al.* Proton-Coupled Electron Transfer in Artificial Photosynthetic Systems. *Acc. Chem. Res.* **51,** 445–453 (2018).

24. Paribok, I. V. *et al.* Tailoring a Tyrosine-Rich Peptide into Size- and Thickness-Controllable Nanofilms. *ACS Omega* **3,** 3901–3907 (2018).

25. Jang, H. S. *et al.* Tyrosine-mediated two-dimensional peptide assembly and its role as a bio-inspired catalytic scaffold. *Nat. Commun.* **5,** 1–11 (2014).

26. Min, K. I. *et al.* Facile Nondestructive Assembly of Tyrosine-Rich Peptide Nanofibers as a Biological Glue for Multicomponent-Based Nanoelectrode Applications. *Adv. Funct. Mater.* **28,** 1–8 (2018).

27. Riley, P. A. Melanin. *Int. J. Biochem. Cell Biol.* **29,** 1235–1239 (1997).

28. Wünsche, J. *et al.* Protonic and electronic transport in hydrated thin films of the pigment eumelanin. *Chem. Mater.* **27,** 436–442 (2015).

29. Partlow, B. P., Applegate, M. B., Omenetto, F. G. & Kaplan, D. L. Di-

tyrosine crosslinking in designing biomaterials. *ACS Biomater. Sci. Eng.* **2,** 2108–2121 (2016).

30. Amdursky, N., Wang, X., Meredith, P., Bradley, D. D. C. & Stevens, M. M. Long-Range Proton Conduction across Free-Standing Serum Albumin Mats. *Adv. Mater.* **28,** 2692–2698 (2016).

31. Ordinario, D. D. *et al.* Bulk protonic conductivity in a cephalopod structural protein. *Nat. Chem.* **6,** 596–602 (2014).

32. Amit, M. *et al.* Measuring Proton Currents of Bioinspired Materials with Metallic Contacts. *ACS Appl. Mater. Interfaces* **10,** 1933–1938 (2018).

33. Mazzuca, J. W. & Schultz, C. P. Quantum Mechanical Enhancement of Rate Constants and Kinetic Isotope Effects for Water-Mediated Proton Transfer in a Model Biological System. *J. Phys. Chem. A* **121,** 819–826 (2017).

34. Edwards, S. J., Soudackov, A. V, Hammes-schiffer, S. & Pennsyl, V. Analysis of Kinetic Isotope Effects for Proton-Coupled Electron Transfer Reactions. *J.Phys.Chem.A* **113,** 2117–2126 (2009).

35. Chernyshev, A., Pomès, R. & Cukierman, S. Kinetic isotope effects of proton transfer in aqueous and methanol containing solutions, and in gramicidin A channels. *Biophys. Chem.* **103,** 179–190 (2003).

36. Ravensbergen, J. *et al.* Kinetic isotope effect of proton-coupled electron transfer in a hydrogen bonded phenol–pyrrolidino[60]fullerene. *Photochem. Photobiol. Sci.* **14,** 2147–2150 (2015).

37. Nagle, J. F. & Tristram-Nagle, S. Hydrogen bonded chain mechanisms for proton conduction and proton pumping. *J. Membr. Biol.* **74,** 1–14 (1983).

38. Mandala, V. S., Liao, S. Y., Kwon, B. & Hong, M. Structural Basis for Asymmetric Conductance of the Influenza M2 Proton Channel Investigated by Solid-State NMR Spectroscopy. *J. Mol. Biol.* **429,** 2192–2210 (2017).

39. Zhong, C. *et al.* A polysaccharide bioprotonic field-effect transistor. *Nat. Commun.* **2,** 1–4 (2011).

40. Josberger, E. E. *et al.* Proton conductivity in ampullae of Lorenzini jelly. *Sci. Adv.* **2,** 1–6 (2016).

41. Sone, Y. Proton Conductivity of Nafion 117 as Measured by a Four-Electrode AC Impedance Method. *J. Electrochem. Soc.* **143,** 1254–1259 (1996).

42. Nguyen, N. T. T. *et al.* Three-Dimensional Metal-Catecholate Frameworks and Their Ultrahigh Proton Conductivity. *J. Am. Chem. Soc.* **137,** 15394–15397 (2015).

43. Kreuer, K. D. Proton-Conducting Oxides. *Annu. Rev. Mater. Res.* **33,** 333–

359 (2003).

44. Boysen, D. A., Uda, T., Chisholm, C. R. I. & Haile, S. M. High-Performance Solid Acid Fuel Cells Through Humidity Stabilization. *Science (80-.).* **303,** 68–70 (2004).

45. Yoo, H. I. & Lee, J. H. Correlation of the cationic 'charge of transport' with the nonstoichiometry and the oxygen exponents in Co1δO. *J. Phys. Chem. Solids* **57,** 65–73 (1996).

46. Riess, I. Mixed ionic–electronic conductors—material properties and applications. *Solid State Ionics* **157,** 1–17 (2003).

47. Yoo, H. I. & Lee, C. E. Conductivity relaxation patterns of mixed conductor oxides under a chemical potential gradient. *Solid State Ionics* **180,** 326–337 (2009).

48. Maier, J. Nanoionics: ion transport and electrochemical storage in confined systems. *Nat. Mater.* **4,** 805–815 (2005).

49. Nakayama, M., Ohshima, H., Nogami, M. & Martin, M. A concerted migration mechanism of mixed oxide ion and electron conduction in reduced ceria studied by first-principles density functional theory. *Phys. Chem. Chem. Phys.* **14,** 6079–6084 (2012).

50. Lee, D. K. & Yoo, H. I. Electron-ion interference and onsager reciprocity in

mixed ionic-electronic transport in TiO2. *Phys. Rev. Lett.* **97,** 3–6 (2006).

51. Lee, D. K. & Yoo, H. I. Measurement of the Onsager coefficients of mixed ionic-electronic conduction in oxides. *Phys. Rev. B - Condens. Matter Mater. Phys.* **75,** 1–5 (2007).

52. Chatzichristodoulou, C., Park, W.-S., Kim, H.-S., Hendriksen, P. V. & Yoo, H.-I. Experimental determination of the Onsager coefficients of transport for Ce(0.8)Pr(0.2)O(2-delta). *Phys. Chem. Chem. Phys.* **12,** 9637–9649 (2010).

53. Xiong, Y.-P. *et al.* Electronic Conductivity of CeO[sub 2]: Its Dependence on Oxygen Partial Pressure and Temperature. *Electrochem. Solid-State Lett.* **13,** B21–B24 (2010).

54. Yoo, H. I. & Kim, H. S. Complete representation of isothermal mass and charge transport properties of mixed ionic electronic conductors. *Solid State Ionics* **225,** 166–171 (2012).

55. Lee, T. & Yoo, H. I. Partial conductivities and Onsager transport coefficient matrix of BaCo0.70Fe0.22Nb0.08O3-?? *Solid State Ionics* **241,** 5–11 (2013).

56. Hong, J. & Yoo, H. Cross effect between ion and electron flows in Fe 3-δ O 4. *J. Mater. Res.* **17,** 1213–1219 (2002).

57. Wagner, C. Equations for transport in solid oxides and sulfides of transition metals. *Prog. Solid State Chem.* **10,** 3–16 (1975).

58. Huggins, R. A. Simple method to determine electronic and ionic components of the conductivity in mixed conductors a review. *Ionics (Kiel).* **8,** 300–313 (2002).

59. Paul, D. K., McCreery, R. & Karan, K. Proton Transport Property in Supported Nafion Nanothin Films by Electrochemical Impedance Spectroscopy. *J. Electrochem. Soc.* **161,** F1395–F1402 (2014).

60. Jiang, S. P. Functionalized mesoporous structured inorganic materials as high temperature proton exchange membranes for fuel cells. *J. Mater. Chem. A* **2,** 7637–7655 (2014).

61. Tsampas, M. N., Pikos, A., Brosda, S., Katsaounis, A. & Vayenas, C. G. The effect of membrane thickness on the conductivity of Nafion. *Electrochim. Acta* **51,** 2743–2755 (2006).

62. Josberger, E. E., Deng, Y., Sun, W., Kautz, R. & Rolandi, M. Two-terminal protonic devices with synaptic-like short-term depression and device memory. *Adv. Mater.* **26,** 4986–4990 (2014).

63. Ramdutt, D. *et al.* Low energy plasma treatment of Nafion®membranes for PEM fuel cells. *J. Power Sources* **165,** 41–48 (2007).

64. Kim, J. H. *et al.* Surface modification of nafion membranes using atmospheric-pressure low-temperature plasmas for electrochemical applications. *Plasma Process. Polym.* **5,** 377–385 (2008).

65. Pham, M. H. & Barz, D. P. J. Bonding Nafion®with polydimethysiloxane: A versatile approach towards ion-exchange membrane microfluidic devices. *J. Memb. Sci.* **537,** 310–314 (2017).

66. Li, X., Zhang, H., Mai, Z., Zhang, H. & Vankelecom, I. Ion exchange membranes for vanadium redox flow battery (VRB) applications. *Energy Environ. Sci.* **4,** 1147–1160 (2011).

67. Daiko, Y., Katagiri, K. & Matsuda, A. Proton conduction in thickness-controlled ultrathin polycation/ nafion multilayers prepared via layer-by-layer assembly. *Chem. Mater.* **20,** 6405–6409 (2008).

68. Fuller, T. F. Experimental Determination of the Transport Number of Water in Nafion 117 Membrane. *J. Electrochem. Soc.* **139,** 1332–1337 (1992).

69. Park, J. S., Jeong, J. K., Chung, H. J., Mo, Y. G. & Kim, H. D. Electronic transport properties of amorphous indium-gallium-zinc oxide semiconductor upon exposure to water. *Appl. Phys. Lett.* **92,** 34–36 (2008).

70. Alam, A. U., Howlader, M. M. R. & Deen, M. J. The effects of oxygen plasma and humidity on surface roughness, water contact angle and hardness of silicon, silicon dioxide and glass. *J. Micromechanics*

Microengineering **24,** 1–14 (2014).

71. Asay, D. B. & Kim, S. H. Evolution of the adsorbed water layer structure on silicon oxide at room temperature. *J. Phys. Chem. B* **109,** 16760–16763 (2005).

72. Wu, B. *et al.* Oriented MOF-polymer composite nanofiber membranes for high proton conductivity at high temperature and anhydrous condition. *Sci. Rep.* **4,** 1–7 (2014).

국문 초록

생물학적 시스템 속에서의 수소 이온 및 전자 전달은 수소 이온/전자 결합 전달 메커니즘에 의하여 조절된다. 수소 이온/전자 결합 전달 메커니즘을 통하여 수소 이온과 전자의 전달은 수평 또는 수직 방향으로 일어날 수 있고 동시에 혹은 순차적으로 수소 이온과 전자의 전달이 이루어질 수 있다. 생명체 속에서 먼 거리 전자 전달과 짧은 거리 수소이온 전달을 함께 조절하는 산화환원 보조인자로서는 다양한 작용기와 그에 따른 기능성을 가진 단백질/펩타이드 복합체가 널리 사용된다. 다양한 종류의 아미노산 중에서 특히 자연계는 다양한 반응에서 산화환원 보조인자로서 타이로신을 택하였다. 가장 널리 알려진 타이로신의 동시의 수소 이온 그리고 전자 전달 현상은 광합성의 명반응에서의 전자 전달과정이다. 망간 칼슘 클러스터에서 엽록소로 전자를 전달하는 과정에서 타이로신이 이 과정을 매개하고 전자 전달과 동시에 타이로신의 작용기 페놀에 있는 수소이온이 수소결합을 하고 있는 히스티딘으로 전달된다. 이 특별한 수소 이온/전자 결합 전달 과정을 통해 단순히 전자 전달 과정만 있을 때에 비하여 200배 정도 빠른 전자 전달이 이루어진다.

전기를 사용하는 소자의 개발은 주로 전자에 의한 전류를 조절하는 것에 초점을 두어왔다. 그러나 자연계 시스템에서 대부분의 전기

신호 전달 과정에는 수소 이온과 같은 여러 이온들의 전달이 관여하고 있으며 이러한 중요성이 대두되며 현재는 수소 이온을 사용한 소자에 대한 수많은 연구들이 진행되고 있다. 더 나아가 자연계에서의 굉장히 효율적인 전하 전달 방식인 수소 이온/전자 결합 전달을 고려하였을 때, 이 메커니즘을 사용하는 시스템을 개발 그리고 그 전달 특성을 조절하는 것은 아마도 후세대 소자 발전의 핵심 열쇠가 될 것이다. 최근 우리 연구실에서는 자연계의 타이로신의 수소 이온 및 전자 전달 특성을 포함한 여러 우수한 특성을 활용하고자 타이로신이 다량 포함된 짧은 펩타이드 시퀀스를 사용하여 하이브리드 필름을 개발하였다. 산화제인 과망간산 칼륨을 사용하여 다이타이로신 결합을 유도하였고 그 결과 펩타이드 필름과 친수성 망간 산화물 하이브리드 필름이 형성되었다. 이 필름은 상온에서 작용하는 다른 바이오 재료에 비해 높은 전도도를 보였는데 이는 미래 생체 전자 소자로서의 활용 가능성이 높을 것으로 예상된다. 또한 수소 이온의 동위 원소인 중수소 이온을 사용하여 확인한 속도론적 동위 원소 효과의 값이 3.3 정도로 일반적으로 알려진 수소 이온의 도약 전도에서의 값인 1.4보다 큰 값을 보였다. 아마도 이는 일반적인 수소 결합 네트워크를 통한 수소 이온의 도약 전도 이외에 자연계 시스템과 같이 수소 이온/전자 결합 전달에 의한 결과일 것으로 예상이 된다. 수소 이온/전자 결합 전달의 속도론적 동위 원소 효과를 수치화 한 값은 온도,

전자 구조의 재배열 에너지, 수소이온 주개-받개 간의 거리 등의 영향을 받아 큰 범위의 값을 갖는다. 따라서 우수한 특성의 하이브리드 필름의 적절하게 활용을 하기 위해서는 실질적인 활용에 앞서, 수소 이온/전자 결합 전달에서의 전하 전달 방식에 대한 연구 및 그에 따른 깊은 이해가 우선되어야 할 것이다.

무기물 재료에서 상당한 양의 이온과 전자가 동시에 전달되는 물질을 혼합 이온/전자 전도체라 부른다. 혼합 이온/전자 전도체에 관한 연구는 오랫동안 진행되어 왔고 전하 간 서로의 움직임에 영향을 주지 않는다는 오랜 법칙은 항상 적용되지 않으며 그들의 서로에 대한 영향은 온도나 비화학량론에 따라 변함이 확인되었다. 이러한 전자와 이온의 간섭 현상은 여러 연구들에서 온상가 계수를 사용하여 보고되었다. 선형 수송 이론에 따르면 전하 운반자의 흐름과 다른 전하 운반자들의 이동 원동력 사이의 계수를 온상가 계수로 정의한다. 또한 두 종류 전하 운반자들이 있는 시스템에서 온상가 계수를 사용하여 네 개의 수송 매개 변수들이 정의된다. 전하 운반자들의 부분 전류나 전기화학적 포텐셜 기울기를 측정하고 조절하면서 다양한 산화물 혼합 이온/전자 전도체의 수송 매개 변수들과 온상가 계수를 구하고자 하는 연구가 다양하게 진행되어 왔고 이를 통해 전하 운반자 간의 간섭 현상을 수치화하고 해석하였다.

넓은 의미에서 혼합 이온/전자 전도체는 수소 이온/전자 결합 전달을 포함한다. 이는 앞서 설명된 무기물 시스템을 플랫폼으로 삼아 수소 이온/전자 결합 전달 메커니즘 연구가 될 수 있음을 암시한다. 따라서 본 연구에서는 앞서 우리 연구실에서 개발한 하이브리드 필름에서의 수소 이온/전자 결합 전달에 대한 연구를 위하여 무기물 시스템에서와 동일하게 온상가 계수와 수송 매개 변수라는 개념을 도입함으로서 벌크 물질의 수소 이온/전자 결합 전달 시스템을 확인하고 수치화 할 수 있는 새로운 패러다임을 제시하고자 한다. 무기물 시스템에서와 동일하게 하이브리드 필름을 사용하여 전극에서 수소 이온의 움직임을 막는 샘플을 제작을 하였고 그 결과 우수한 수소 이온 전도체인 나피온 막을 사용하여 전자의 간섭 현상으로 인해 움직이는 수소 이온과 균형을 이루는 수소 이온의 전기화학적 포텐셜 기울기가 측정되었다. 두 개의 수송 매개 변수들도 계산되었고 이를 통해 거시적인 필름 샘플에서의 수소 이온 하나와 전자 하나의 결합된 전도 현상을 확인할 수 있었다. 또한 동위원소인 중수소 이온을 사용한 전도 현상 연구도 타이로신 포함 펩타이드/망간 산화물 하이브리드 필름에서의 수소 이온/전자 결합 전달 현상을 재현하였다.

주요어 : 수소 이온/전자 결합 전달, 혼합 이온/전자 전달체, 온상가 계수, 나피온, 수송 매개 변수, 타이로신 포함 펩타이드/망간 산화물 하이브리드 필름

학번 : 2017-24715

감사의 글

2년 동안 즐겁고 보람찬 연구실 생활을 할 수 있도록 저를 지도해주시고 응원해주신 모든 분들께 감사의 말씀 드립니다.

가장 먼저 항상 관심을 가져주시고 신경 써주신 저의 지도 교수님 남기태 교수님께 진심으로 감사드립니다. 연구에 있어서 어려움도 많았지만 교수님의 꼼꼼한 지도와 진심 어린 격려로 용기를 가지고 앞으로 나아갈 수 있었습니다. 교수님께서 해주신 말씀 중 가장 기억이 남은 말이 있습니다. 이 연구는 내가 아니면 할 수 없도록, 나만의 강점을 살려야 한다. 결코 쉬운 것은 아니지만 사실 정말 중요한 이야기라 생각이 들고 제가 앞으로 살아가며, 연구를 해 나가며, 또 때론 지쳐있을 때 저를 앞으로 나아가게 하는 큰 원동력이 될 것이라 생각됩니다. 교수님의 가르침 모두 마음 속에 소중히 간직하고 훌륭하고, 또 좋은 사람으로 성장할 수 있도록 하겠습니다. 정말 감사드립니다.

저의 석사 학위논문 심사를 맡아주신, 그리고 두 분께서 기억하실지는 모르겠지만 2년 전 대학원 입학면접에서도 심사를 맡아 주셨던 김미영, 선정윤 교수님께 진심으로 감사드립니다. 김미영 교수님, 학부 때 교수님께서 무엇이든 2-3년은 해 보아야 이 일이 적성에 맞는지 정

확히 말할 수 있으며 해보지 않고는 말하지 못한다고 말씀하셨던 것이 당시 정말 와 닿았고 지금까지도 잊혀지지 않습니다. 저의 멋진 인생 선배님께, 꼭 교수님처럼 좋은 사람으로 성장하겠다 약속 드립니다. 또, 흔쾌히 학위 심사를 맡아 주신 선정윤 교수님, 학위 심사 발표에서 연구에 대해 많은 조언 주시고 수고했다 격려해주셔서 정말 감사드립니다. 아직도 많이 부족한 저이지만 앞으로 꾸준히 성장해 나가도록 하겠습니다. 많은 관심 부탁드립니다.

2년간 함께 과제를 진행 해주시고 많은 조언 주신 이윤식, 그리고 권장연 교수님께도 진심으로 감사드립니다. 두 교수님께 제 연구를 확인 받으며 무엇이 부족한지, 어떻게 극복할 수 있을지 정말 많은 도움이 되었습니다. 너무 감사드리고 앞으로 쭉 지켜봐 주시면 꼭 훌륭하게 성장하겠습니다. 또 함께 연구 공유하고 디스커션 했던 남궁석, 그리고 송민규 두 착하고 똑똑하고 또 사실 재미있었던 오빠분들께 진심으로 감사드리며 앞으로도 좋은 인연 쭉 이어 나갔으면 좋겠습니다.

매일 얼굴보고 부딪히며 그 시간을 너무 행복하고 소중하게 만들어준 연구실 식구들께 진심으로 감사드리며 짧게 글 올립니다. 먼저 알콩달콩(?) 펩타이드 팀 식구들께, 우리의 영원한 수장님 재훈 오빠와 그런 그를 트위저로 쓰는 욱현이(그리고 꽃보다 누나의 이승기..(?)), 나

때문에 고생 정말 많았는데 진짜 진심으로 고맙고 각자 다른 길을 걸어가도, 이름만 펩타이드 팀이라도 항상 연락하고 회식도 자주 합시다. 2년간 항상 내 옆자리를 지켰던 영혜 언니, 회식 때 나를 껴안으며 재훈 오빠 혼낼 때 감동 받았어요. 기동 오빠가 졸업 때 유언처럼 '미송아 영혜가 많이 도와 줄거야'라고 하고 나갔었는데 아셨나요. 진짜 언니 항상 너무 고맙고 사랑해요(이미 졸업하신 양기동 박사님께도 감사의 말씀드립니다ㅎ). 내가 연구실 들어올 때 학위 모자 즐거워서 하늘로 던져 놓고서 그 이후 계속 함께한 혜은 언니, 못난 후배들 감싸주는 천사 같은 언니 진짜 고맙고 앞으로는 매일매일 웃을 일만 있길 바랄게요(일본 가면 꼭 언니 찾아갈게요!). 진정한 강력한 멘탈의 소유자 윤영 언니, 언니랑 있으면 우울해도 항상 즐거워졌고 나도 언니처럼 주변을 즐겁게 할 수 있는 사람이 되고 싶다 항상 생각합니다. 언니에게 쌍따봉을bb. 나와 함께 꽃보다 누나 찍어준 혜온 언니, 내가 남자였으면 난 언니에요 알죠? 나 나가도 같이 놀아줘 우리 우정 영원히!(집착) 나의 학부 시절까지 모든 걸 꿰뚫고 있는 정으니, 학부 때 우리 친했냐고 음해하려는 세력(ex. 준호장)에게, 지금 만큼 친하지는 않았다 인정합니다. 근데 지금은 나중에 오랜만에 연구실을 찾아오면 정으니를 먼저 찾을 만큼 진짜 친합니다. 언니, 내가 진짜 언니 좋아하는 거 알겠지만 또 알아줘. 너무 착하고 난

관에 부딪힐 때 도움 많이 주신 희윤 오빠, 언제나 친절하게 대하고 함께 고민해주시고 도와주셔서 정말 감사드려요. 재주 많고 언제나 친절한 정석 오빠, 사실 초반에 낯을 많이 가리는데 오빠가 먼저 다가와서 내 맘속의 얼음을 빠르게 녹여줘서 더 빠르게 연구실에 적응할 수 있었던 것 같아요. 늘 땡큐입니다. 항상 웃으며 대답해주는 홍민 오빠, 당연히 할 부탁들도 매번 미안하다고 하시고 진짜 오빤 천사에요. 군대에서도 분명 천사 조교였을거야... 수많은 후배들의 정신적 지주이자 자기가 더 대단하면서 자꾸 너희 대단하다 하면서 격려해주는 승학 오빠, 오빠 진짜 멋있고 대단하고 좋은 사람입니다. 또다른 수많은 후배들의 정신적 지주이자 매사 진지하게 후배들을 도와주는 효용 오빠, 오빠의 그 차분한 목소리가 마음의 안정을 주는 거 아시나요. 오빠에게도 쌍따봉을. 솔직히 처음엔 무서웠지만 이제는 별로.. 상원 오빠, 장난이고요(?). 오빠가 연구실에 신경을 많이 써 주시는 것 같아 항상 감사해요. 아직도 엠티에서의, 사극에 나올법한 수염 작품이 잊혀지지 않는 경도 오빠, 미친 듯이 친 배드민턴까지, 제 소확행 실현을 도와주셔서 정말 감사드립니다. 다른 선배들과는 다르게 초반에 존댓말로 나를 대하던 승우 오빠, 존댓말이 너무 임팩트가 컸던 탓인지는 모르겠으나 이제는 편하게 반말 하는, 술자리에서 선배들한테 충성충성 외치는 오빠일지라도 진짜 편하답니다. 함께 또 많이 고생한 따뜻한 헌진 오빠, 그 시절 생각에 애잔하네요 오

빠 꼭 행복하세요. 좋은 사람에게 꼭 복이 옵니다. 조삼모사라는 말에 나도 모르게 음 맞는 거 같아 인정하게 되는 강희 오빠, 그만큼 오빠는 그 누구보다도 후배들과 친하게 지내고 많이 베풀고 주변을 즐겁게 하는 좋은 사람이에요. 오빠도 복 많이 받을 거에요. 항상 나에게 밝게 대해 주고 재채기때마다 bless you 해주는 샘 오빠, '빈' 오빠도 남은 기간 알차고 보람찼으면 좋겠어요. 계속 연락해요! 벌서 들어온 지 한 학기 넘은 원일 오빠, 오빠도 앞으로 잘 나아가리라 믿습니다. 좋은 연구실 생활 하세요. 소문으로는 drinking 하면 폭주한다는 윤호야, 두렵지만 그래도 언젠가 한 번쯤은 같이 놀고 싶다는 생각은 항상 가진다. 나중에 언제 한 번 불러줘. 나의 친구의 친구(?후배?) 뭐튼 이제는 나의 진짜 좋은 친구인 령명아, 보아하니 너가 골드팀 짱인거 같은데 우리 언니 오빠들 잘 부탁한다 무섭지 않게 잘해드려. 착하고 유쾌하고 안한다면서 할거 다하는 프레디 무큐리 오빠, 잊지 못할 거에요. 힘들고 우울할 때 가장 먼저 떠오를 장면 감사드립니다. Dr. Bala and Dr. Saran, it was an honor to meet you and share my research with you. I would never forget my life here in BMNL with you. Thank you. 아무리 미워하려 해도 미워할 수 없는 4명의 나의 동기 오빠님들께 진심으로 감사하며 하고 싶은 말은 많지만 짧게 글 전합니다. 엄마와 아빠 그 사이 어딘가의 남헌 오빠, 친동생처럼 아껴주고 힘들 때 위로해주고 또 재미있게 놀아

주고 챙겨주고 정말 고마워요. 진짜 그리울 거야. 사촌 오빠 같은 준호 오빠, 솔직히 같은 연구실 했을 때 망했다라고 생각했었는데 지금은 오빠 둘도 없는 최고의 친구에요. 친해지고 조언도 많이 듣고... 죽이 잘 맞아서 기분이 좋았네요. 친 오빠 같기도 베프 같기도 한 강규 오빠, 나와 맞는 오빠의 그 저렴한 개그 취향 덕에 많이 친해졌네요. 내가 오빠 못생겼다고 틱틱대고 시비 털어도 항상 받아줘서 고마워요. 마지막으로 자꾸 말 걸고 괜히 놀리면 반응 너무 좋은 오랜 친구 탁래 오빠, 졸업 후 '뭐요' 탁래 꼭 돌아와줘요. 그리고 앞으로는 제발, 카톡 읽씹도 좋으니 많이 소통합시다~. 윤영언니가 질투해도 우리 다섯 자주 인연을 이어 나갔으면 좋겠습니다. 연구실 사람이 너무 많아 옆에서 '그 외 잡다한 떨거지들에게 안녕을 고한다'라고 쓰라는 옆자리 남성분의 유혹에도 불구하고 여러분들께 고마운 것이 많아서 참고 썼습니다. 비록 졸업하여 나가지만 계속해서 연락하고 살았으면 좋겠어요. 연락주세요~~

마지막으로 내가 무엇을 하든 항상 서포팅 해주겠다는 아빠, 딸 걱정은 하나 항상 믿어주는 엄마, 비슷한 길을 걸어왔기에 그 누구보다 날 잘 이해하는 오빠에게 응원 진심으로 감사드립니다.

2년 간 잊지 못할 추억을 주신 모든 분들께, 모두들 행복하세요!